R-06-100

Regional groundwater flow model for a glaciation scenario

Simpevarp subarea – version 1.2

O Jaquet, P Siegel
Colenco Power Engineering Ltd

October 2006

Svensk Kärnbränslehantering AB
Swedish Nuclear Fuel
and Waste Management Co
Box 5864
SE-102 40 Stockholm Sweden
Tel 08-459 84 00
+46 8 459 84 00
Fax 08-661 57 19
+46 8 661 57 19

ISSN 1402-3091
SKB Rapport R-06-100

Regional groundwater flow model for a glaciation scenario

Simpevarp subarea – version 1.2

O Jaquet, P Siegel
Colenco Power Engineering Ltd

October 2006

Contents

1 Introduction

In the framework of the safety assessment SR-Can, SKB needs to demonstrate that a repository in crystalline rock will meet the long-term safety requirements set forth by the authorities. At the time scale of the safety assessment (i.e. 10^5 to 10^6 a), climatic changes are expected that will modify subsurface conditions. Therefore, the potential impact of climatic changes has to be evaluated with respect to repository performance and safety.

In particular, climatic changes with expanding ice sheets are likely to occur. The growth and decay of ice sheets will affect the groundwater flow field and its composition. For this reason, these (long term) transient glacial effects have to be considered when studying groundwater flow at a regional scale. For assessment purposes it is necessary to develop a numerical model of the groundwater flow for a glaciation scenario. This groundwater flow model is the subject of this study.

2 Objectives

The present study was established on the basis of SKB technical specifications. Its main objective is to evaluate the groundwater velocity and salinity fields for the different conditions prevailing during a glaciation period, including specific sensitivity cases.

Another specific objective is the evaluation of repository performance for periods of glaciation and deglaciation. In particular, the flow paths from repository depth to the surface need to be assessed for different glacial conditions to evaluate relative differences in solute travel-times.

The report begins with an account of the modelling approach applied. Then, the results of the different cases simulated are described, analysed and interpreted in detail. Finally, conclusions are drawn up together with some recommendations related to potential modelling issues for the future.

3 Modelling approach

3.1 Conceptual model

The conceptual model Simpevarp 1.2 (Simpevarp regional model S1.2; /Hartley et al. 2005/) provides the geological basis for the regional groundwater flow model, i.e. the glaciation model. The S1.2 regional model provides the deterministic deformation zones as well as the rock domain that constitutes the basis for the geometrical framework of the glaciation model. In terms of size, the glaciation model extends far beyond the S1.2 regional model in the northerly and southerly directions.

A stochastic equivalent porous medium approach was selected for the glaciation model. Numerical modelling of variable-density groundwater flow including rock-matrix diffusion is performed at regional scale for a glacial period of approximately 20,000 years whereby the boundary conditions are provided by a dynamic ice sheet model /SKB 2006/.

In ice sheets, the sub-glacial layer is a water conductive layer assumed to exist at the ice/bedrock interface in the area of basal melting. This layer plays a major hydraulic role in carrying meltwater which can then infiltrate in the subsurface where significant modifications of the flow field are to be expected. Due the scarcity of data a stochastic approach was chosen for the description of the conductive features in the sub-glacial layer.

The movement – involving glacial build-up and retreat – of the ice sheet is specified through the use of transient boundary conditions. The existence of the Baltic Sea is neglected, i.e. there are no fluctuations in sea level as well as no supply of salt from the Baltic Sea.

Geomechanical effects due to ice loading likely to induce modifications of the groundwater flow field were not considered as part of the conceptual model. Therefore, the impact of the ice sheet loading in terms of rock deformation leading to variations in porosity, hydraulic conductivity and pore pressure were not included in this modelling approach. In addition, the progression of the ice sheet is assumed to be isothermal; this means that permafrost areas located in the surroundings of the ice sheet were neglected and thus no reduction in hydraulic conductivity was taken into account for these areas (see Figure 3-1).

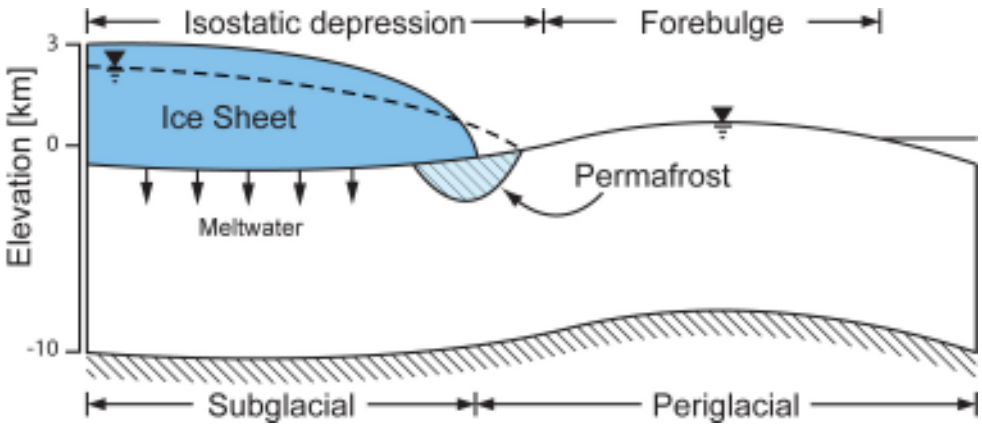

Figure 3-1. *Glaciation conceptual model /after Lemieux 2006/: description of variable-density groundwater flow including rock-matrix diffusion using boundary conditions from a dynamic ice sheet model. Ice loading and permafrost effects were not considered.*

3.2 Model domain

The longest dimension of the 3D domain of the glaciation model extends about 300 km upstream and ca 100 km downstream of the repository location (see Figure 3-2).

The width of the glaciation model is the same as that of the S1.2 regional model (21.6 km). The repository is assumed to be located inside the S1.2 local model domain (7.8×3.2 km). The depth of the glaciation model was set to 2.3 km to match the vertical extent of the S1.2 regional model.

The main orientation of the domain, i.e. its long axis, coincides with the main ice flow direction during the glacial cycle. According to /Näslund 2004/, this orientation ranges predominantly between N180 degrees and N170 degrees East. N180 degrees was therefore ascribed to the main orientation of the glaciation-model domain.

3.3 Deformation zones

The deformation zones, i.e. the fracture zones, corresponding to the Hydraulic Conductor Domains (HCD), of kilometric extent were taken from the S1.2 regional model (see Figure 3-3). They are assumed to intersect the entire thickness of the domain. For the domain of the glaciation model beyond the 21.6×13 km area of the S1.2 regional model, no explicit information on the deformation zones was available in terms of geometric and hydraulic parameters. Therefore, we assume that the spatial-variability characteristics of the equivalent permeability and porosity fields of the S1.2 regional model can be extrapolated by stochastic simulation for the remainder of the glaciation model domain. Since the hydraulic effects of the deformation zones are integrated into these equivalent properties, this means that the entire domain of the glaciation model is considered to contain deformation zones.

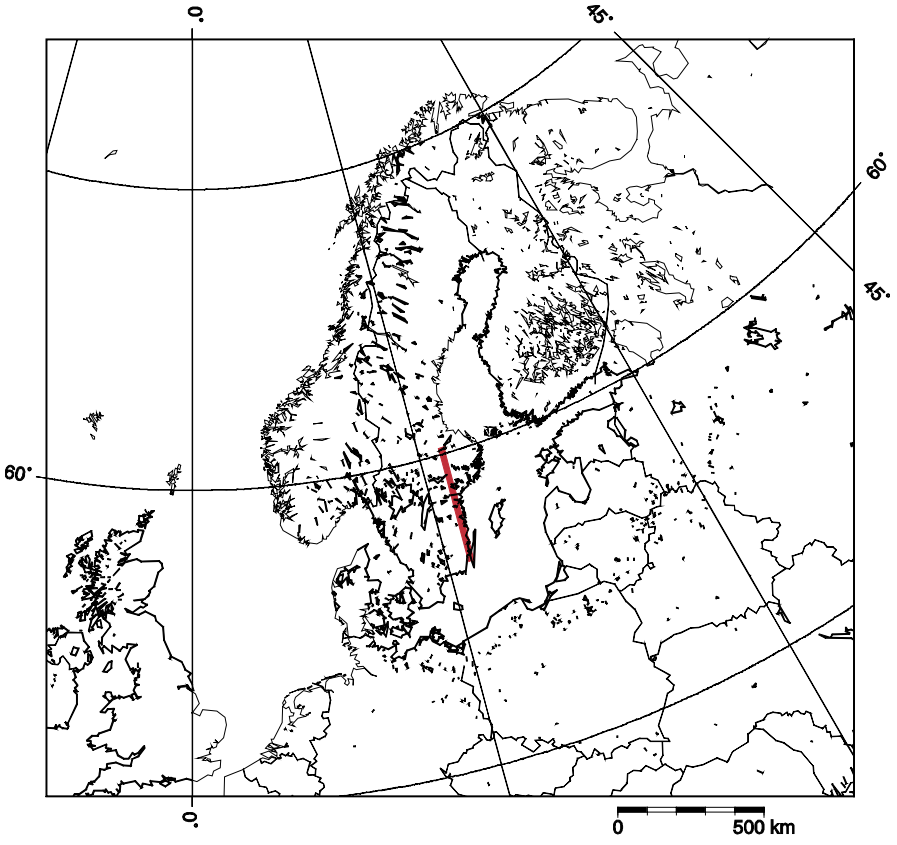

Figure 3-2. *Location of glaciation model (red line).*

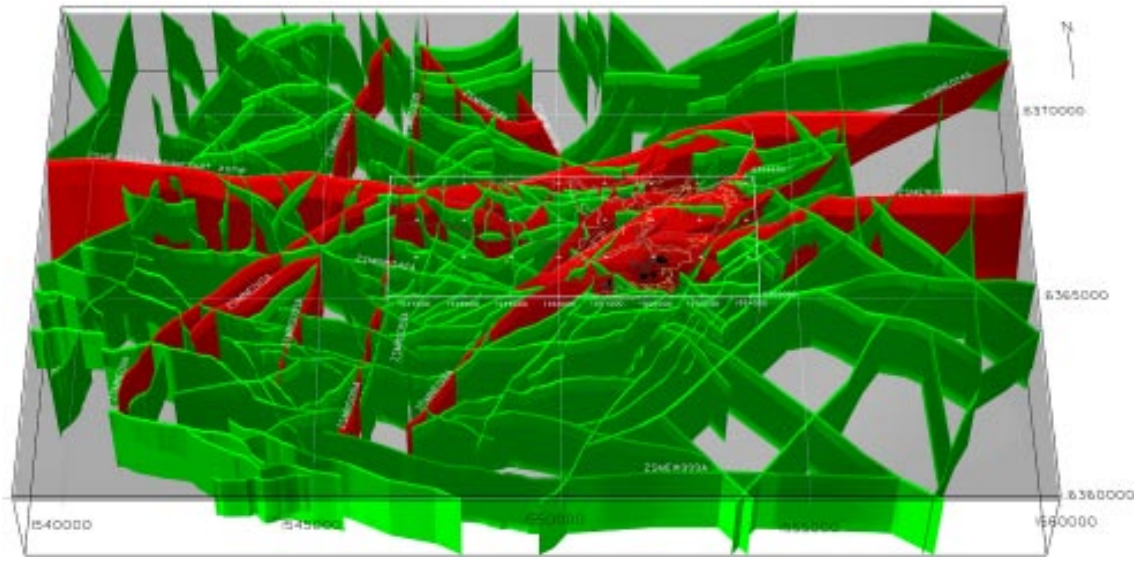

Figure 3-3. *Location and geometry of deformation zones in the S1.2 regional model area of Simpevarp /after Hartley et al. 2005/. Verified deformation zones of high confidence (red) and lineaments of low confidence (green).*

3.4 Phenomenology

For the glaciation model (conceptualised as stochastic equivalent porous medium), the description of density-driven groundwater flow induced by variable salinity of the groundwater in the presence of rock-matrix diffusion is obtained using the following equations implemented in ConnectFlow 8.1 /Hoch and Jackson 2004/.

The flow equations are governed by Darcy's law:

$$\mathbf{q} = -\frac{\mathbf{k}}{\mu}\left(\nabla p^R - (\rho - \rho_0)\mathbf{g}\right) \quad (1)$$

where:

q : Darcy velocity

k : intrinsic permeability tensor

μ: fluid viscosity

p^R: residual pressure with

p: pressure (total)

ρ: fluid density

ρ_0: reference density of fluid (freshwater)

z: elevation

z_0: reference elevation

g: gravitational acceleration.

and the continuity equation:

$$\frac{\partial}{\partial t}(\phi_f \rho) + \nabla \cdot (\rho \mathbf{q}) = 0 \quad (2)$$

where:

φ_f: fracture porosity.

A specific storage coefficient of zero is assumed. This hypothesis is justified given the range of hydraulic conductivity, the value taken for the specific storage (10^{-6} m^{-1}; after /Jaquet and Siegel 2004/) and the time steps considered (cf part 3.5) for the glaciation model.

The representation of salt transport with rock-matrix diffusion is given by:

$$\frac{\partial}{\partial t}(\phi_f \rho c) + \nabla \cdot (\rho \mathbf{q} c) = \nabla \cdot (\phi_f \rho \underline{\underline{D}} \cdot \nabla c) + \zeta \rho D_{int} \frac{\partial c'}{\partial w}\Big|_{w=0} \quad (3)$$

where:

c: concentration of solute flowing through the fractures (expressed as a mass fraction)

$\underline{\underline{D}}$: hydrodynamic dispersion tensor

ζ: flow wetted surface

D_{int}: effective diffusion coefficient

c': concentration of solute in the rock matrix (expressed as a mass fraction)

w: coordinate into the rock matrix.

And the hydrodynamic dispersion tensor is defined as follows:

$$\underline{\underline{D}} = \frac{D_m}{\tau}\delta_{ij} + \alpha_T v \delta_{ij} + (\alpha_L - \alpha_T)\frac{v_i v_j}{v} \quad (4)$$

where:

D_m: molecular diffusion coefficient

τ: tortuosity

α_L, α_T: longitudinal and transverse dispersivity

v: porewater velocity (with $\mathbf{v} = \frac{\mathbf{q}}{\phi}$ and $v = \sqrt{\mathbf{v} \cdot \mathbf{v}}$).

Finally for the rock-matrix diffusion, the following equation is used:

$$\phi_m \frac{\partial}{\partial t}(\rho c) = \frac{\partial}{\partial w}\left(\rho D_{int} \frac{\partial c'}{\partial w}\right) \quad (5)$$

where:

φ_m: rock-matrix porosity

D_{int}: effective diffusion coefficient.

For equation (5), the boundary conditions are the following: (a) the matrix concentration at the fracture surface is equal to the local concentration in the fractures:

$$c'(w = 0) = c \quad (6)$$

and (b) the flux of concentration in the matrix is zero at the maximum depth of penetration into the matrix:

$$-D_{int} \frac{\partial c'}{\partial w}(w = d) = 0 \quad (7)$$

where:

d: matrix diffusion length ($d = \frac{b}{2}$ where b is the fracture spacing and $\zeta = \frac{2}{b}$).

3.5 Numerical aspects

Considering the size of the glaciation model, it was decided to apply a numerical scheme for transient salt transport which is more efficient in terms of CPU time than to solve the fully coupled form of these equations. This scheme corresponds to the approach used for the regional hydrogeological simulations of Simpevarp /Hartley et al. 2005/. It involves a decoupling of the solutions for pressure and salt transport by linearising the equations /Marsic et al. 2002, Hartley et al. 2004/. At each time step the groundwater flow calculations are solved in two stages: (a) solve for flow, accounting for variable density and (b) resolve with advection-dispersion-matrix-diffusion equations for salinity in the new flow field.

The GMRES (Generalized Minimal Residual) iterative solver of NAMMU /Marsic et al. 2001/ is used to solve the flow and transport equations. GMRES is a Krylov-based iterative method for the solution of linear systems associated to unsymmetric matrices. For the time discretisation, a fully implicit Crank-Nicholson transient scheme is used. The matrix diffusion equation is solved using a numerical approach based on a method developed by /Carrera et al. 1998/. The numerical parameters selected for simulation are listed in Table 3-1.

3.6 Flow parameters

The equivalent properties of the Hydraulic Conductor Domains (HCD), Hydraulic Rock Domains (HRD) and Hydraulic Soil Domains (HSD) are taken from the Simpevarp regional model (S1.2: /Hartley et al. 2005/) and correspond to the base case with reference water calibration (case: SReg_4Component_IC2).

The HCD properties are assumed constant for each deformation zone. The deformation zones were downscaled on the grid of the Simpevarp model and then a numerical up-scaling of bedrock fracturing including deformation zones was performed to obtain the equivalent properties for each element of the model. The results are equivalent hydraulic conductivity tensors and porosity values for the Simpevarp area which account for the hydraulic effects of the deformation zones (details can be found in /Hartley et al. 2005/).

For the remainder of the glaciation-model domain beyond the Simpevarp area, the equivalent permeability (diagonal) tensor and porosity fields were extrapolated by stochastic simulation using parameters of spatial variability (such as mean, standard deviation and correlation length) estimated from the Simpevarp area (see Table 3-2).

The properties of the HSD which describe layers of silty till are considered as constant over the whole top surface of the glaciation model. Their values were set equal to those of the Simpevarp area /Hartley et al. 2005/.

The geometry of conductive features (or ice tunnels) in the sub-glacial layer was described using a stochastic model. The geometry of the conductive features was then projected into the glaciation model with a vertical extent corresponding to the thickness of the HSD. The proportion of meltwater likely to flow in the conductive features and in the HSD depends on the transmissivity contrast between these two units. Finally, the hydraulic conductivity of the conductive features was calibrated in such a way that lifting of the ice is avoided. The specific storage was assigned based on previous studies (see also part 3.4): a uniform value of zero for the resulting up-scaled fractured rock domain (HRD+HCD), HSD and sub-glacial layer.

Table 3-1. Numerical parameters.

GMRES convergence criterion	Time stepping	Accuracy parameter for matrix diffusion
10^{-6}	100 a	10^{-4}

Table 3-2. Flow parameters.

Domain (thickness)	Hydraulic conductivity [m/s]	Standard deviation [log 10]	Correlation length [m]	Specific storage [m^{-1}]
HSD_1 (0–1 m)	10^{-5}	Uniform	Uniform	0.0
HSD_2 (1–3 m)	10^{-7}	Uniform	Uniform	0.0
HRD+HCD (3–2,100 m)	[1)] Kxx = $1.7 \cdot 10^{-8}$ [1)] Kyy = $1.9 \cdot 10^{-8}$ [1)] Kzz = $1.4 \cdot 10^{-8}$	0.69 0.65 0.75	[2)] 300+(800, 400, 15,000)	0.0
Bottom (2,100–2,300)	$5.0 \cdot 10^{-10}$	Uniform	Uniform	0.0

[1)] Geometric mean of diagonal component.

[2)] Variogram = isotropic exponential model + anisotropic exponential model.

3.7 Transport and rock-diffusion parameters

The transport and rock-diffusion parameters applied for the glaciation model are given in Table 3-3 and in Table 3-4.

The molecular diffusion coefficient is set equal to 10^{-9} $m^2 \cdot s^{-1}$ and the tortuosity is identical to 1.

Table 3-3. Transport parameters.

Domain	Porosity [–]	Standard deviation [log 10]	Correlation length [m]	α_L [m]	α_T [m]
HSD_1	$5 \cdot 10^{-2}$	Uniform	Uniform	[3)] 80, 160	[3)] 20, 80
HSD_2	$5 \cdot 10^{-2}$	Uniform	Uniform	[3)] 80, 160	[3)] 20, 80
HRD+HCD	[1)] $4.2 \cdot 10^{-5}$	0.85	[2)] 300+(800, 400, 15,000)	[3)] 80, 160	[3)] 20, 80
Bottom	$5.0 \cdot 10^{-5}$	Uniform	Uniform	[3)] 80, 160	[3)] 20, 80

[1)] Geometric mean of fracture porosity.

[2)] Variogram = isotropic exponential model + anisotropic exponential model.

[3)] Values for Simpevarp area.

Table 3-4. Rock-matrix diffusion parameters.

Domain	Effective diffusion coefficient [$m^2 \cdot s^{-1}$]	Flow wetted surface [$m^2 \cdot m^{-3}$]	Rock matrix porosity [–]	Matrix diffusion length [m]
HRD+HCD	$5 \cdot 10^{-13}$	2	$5 \cdot 10^{-3}$	0.5
Bottom	$5 \cdot 10^{-13}$	2	$5 \cdot 10^{-3}$	0.5

3.8 Discretisation

The glaciation model was discretised using a 3D finite-element mesh with cuboid elements (8 nodes) of non-uniform size. Due to ConnectFlow limitations only one nested level could be defined which corresponds to the Simpevarp area. The grid resolution in the horizontal direction is 100 m for the Simpevarp model area and 300 m for the remainder of the glaciation model.

In the vertical direction, the discretisation of the glaciation model is the same as that of the S1.2 regional model and corresponds to a global discretisation of 100 m with metric refinements for the Hydraulic Soil Domains.

The finite-element mesh of the glaciation model was generated with Colenco tools and contains a total of 3,265,920 elements.

For the topography, a uniform elevation of zero was applied to the entire area of the glaciation model. This simplification was required because numerical problems were encountered with ConnectFlow when applying a prescribed recharge on a spatially variable topography.

3.9 Stochastic simulations

Fractured rock domain

The equivalent hydraulic properties for the fractured rock domain (HRD+HCD) of the glaciation model beyond the Simpevarp area were extrapolated with stochastic cosimulation using the turning bands method /Chilès and Delfiner 1999/. The parameters for the cosimulation were estimated using the equivalent hydraulic conductivity and porosity fields from the Simpevarp area.

Variograms and cross variograms were calculated to parameterise all spatial (cross) correlation (see Figure 3-4) between the diagonal components of the hydraulic conductivity tensor and the porosity using a consistent multivariate model composed of a sum of exponential variograms (cf Table 3-2). In addition, the cosimulation of the equivalent hydraulic properties for the glaciation model domain was performed to match the histograms of the hydraulic properties for the Simpevarp area.

Ultimately, every element of the finite-element mesh discretising the fractured rock domain beyond the Simpevarp area was assigned a “stochastic” equivalent hydraulic conductivity and porosity (see Figure 3-5).

Sub-glacial layer

Ice sheets produce large amounts of subglacial meltwater even when growing. In this case, meltwater is due to friction at the ice/bedrock interface and to the geothermal gradient /Paterson 1994/.

The characteristics of ice sheet hydrology were based on conceptual information provided by SKB (see Figure 3-6). In ice sheets, the sub-glacial layer is a water conductive layer assumed to exist at the ice/bedrock interface in the area of basal melting. Upstream of the ELA (Equilibrium line between accumulation and ablation areas), the sub-glacial layer carries the basal meltwater generated at the bottom of the ice sheet. In the ablation area, downstream of the ELA, the sub-glacial layer receives both basal and surface meltwater. Due to the large amount of meltwater at specific locations, erosional conductive features (or ice tunnels) are formed within the sub-glacial layer.

In the ablation area, the pattern of catchment areas was assigned using recent observations of ice sheets in Greenland. Each catchment area has a moulin through which surface meltwater is assumed to be transferred instantaneously to the sub-glacial layer.

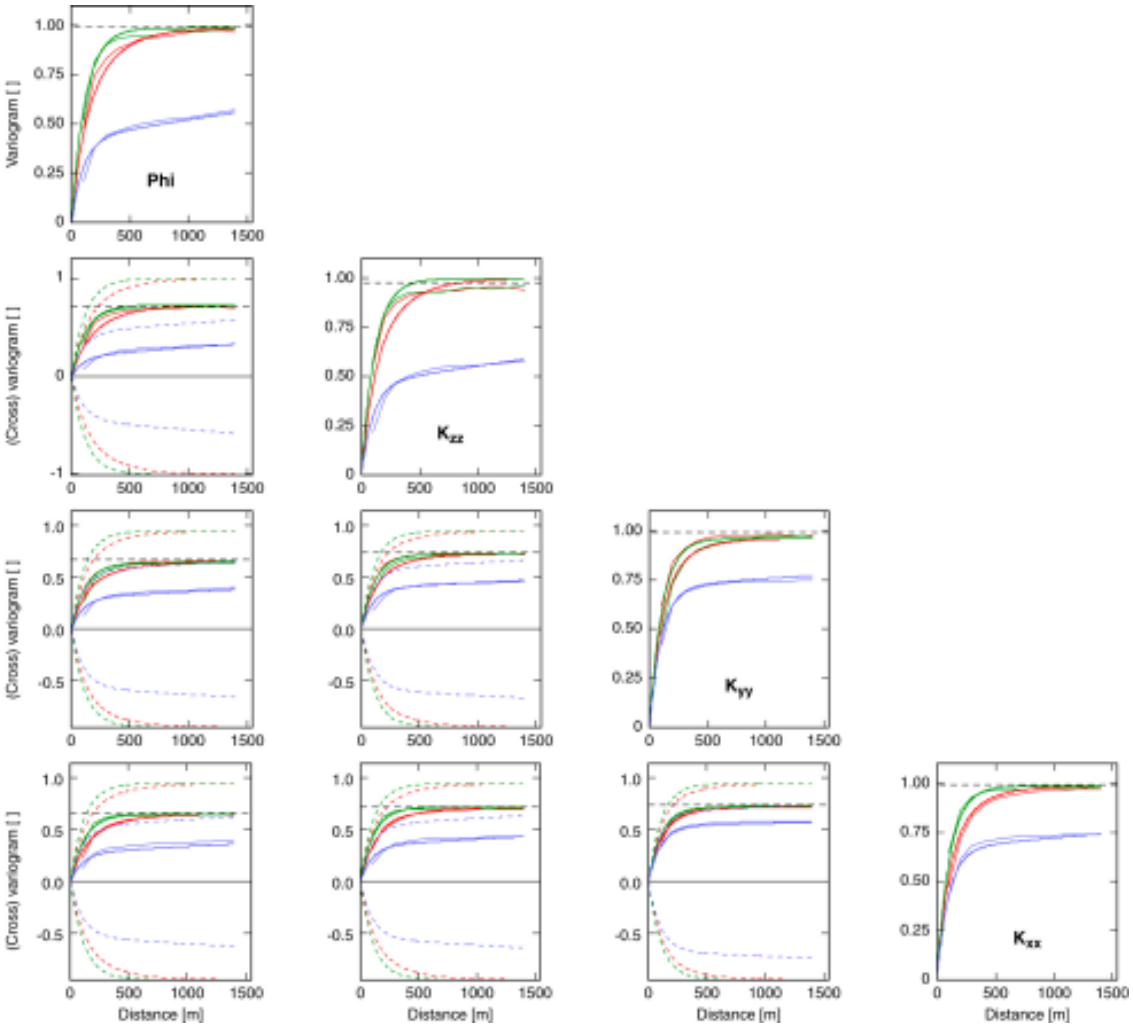

Figure 3-4. *Multivariate anisotropic variogram model (thick curve) fitted to the experimental variograms and cross variograms (light curve) applied for the stochastic cosimulation of equivalent hydraulic properties for the glaciation model domain. Dashed curves correspond to the validity bounds for the fitted cross variograms. The dashed horizontal line represents the variance (or covariance) of the transformed (Gaussian) data.*

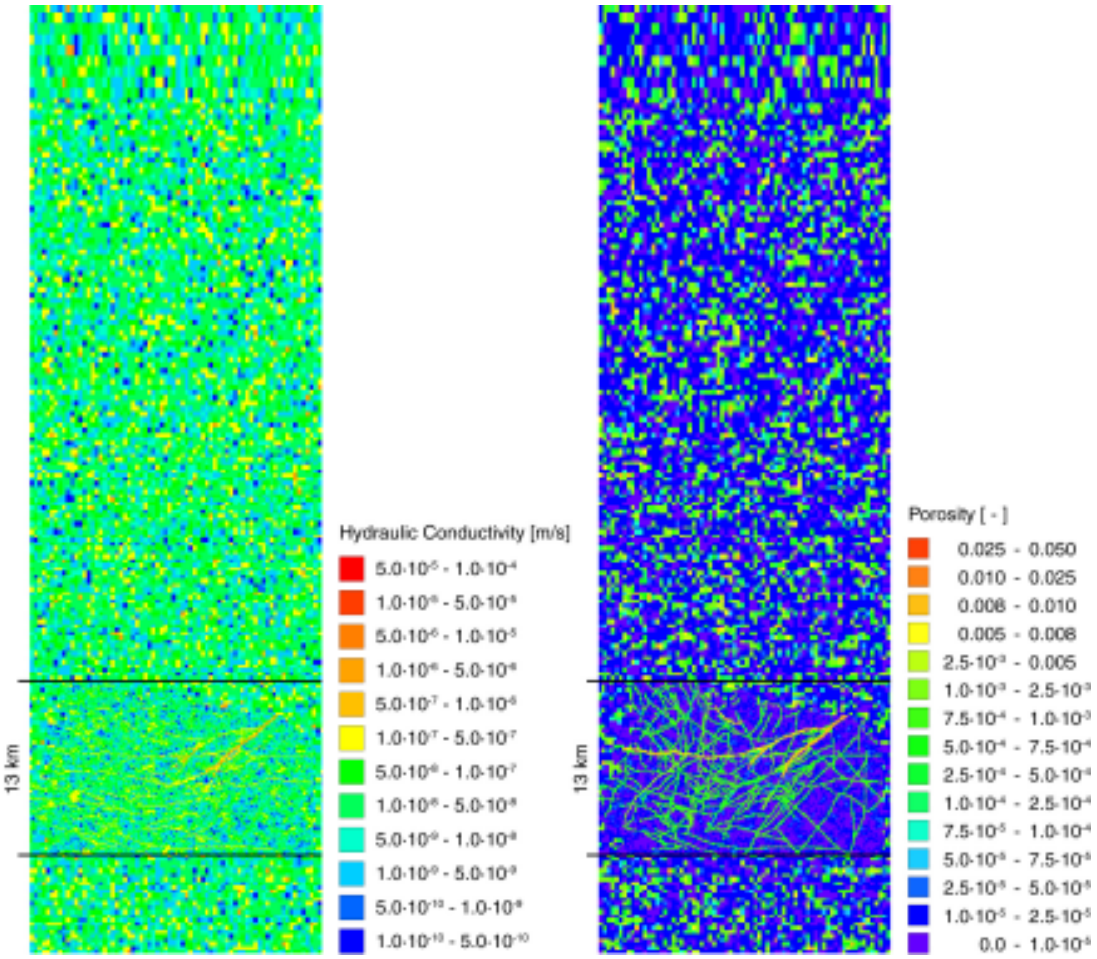

Figure 3-5. *Cosimulation of equivalent hydraulic conductivity (K_{xx}) and porosity for a part of the glaciation-model domain (at a depth of 1,000 m) with the Simpevarp area (of 13 km extent in the South part) showing the discretised deformation zones.*

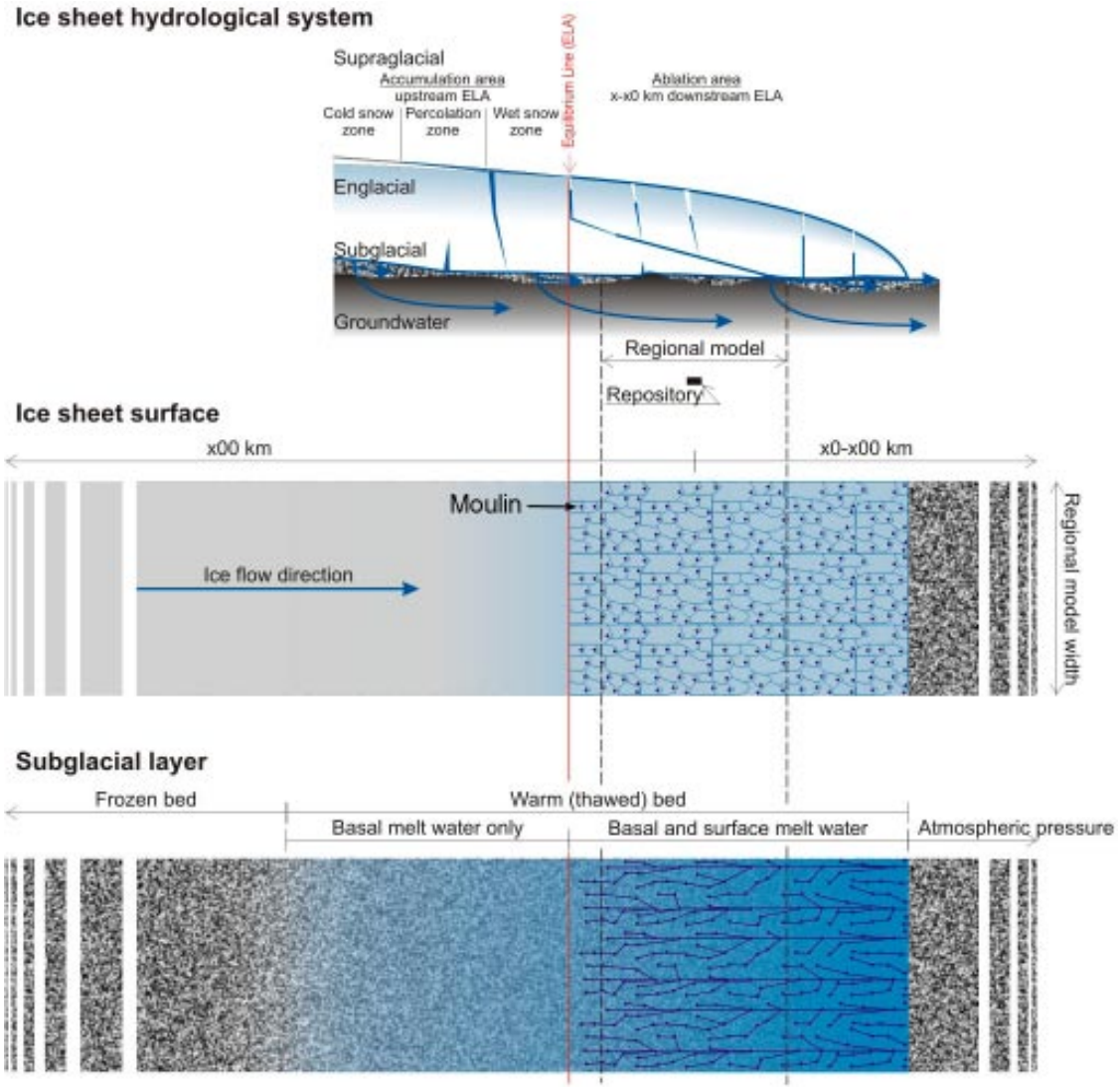

Figure 3-6. *Sub-glacial layer concept /after SKB 2006/.*

The minimum distance between conductive features was estimated based on the average distance (measured perpendicular to the direction of ice flow) between moulins (see Figure 3-7). The maximum distance was set equal to the distance between eskers typically encountered in Sweden. Therefore, the separation distance for the conductive features was considered to range between 3 and 10 km.

Information on the location of conductive features in a sub-glacial layer currently remains speculative. Therefore, the geometry of conductive features was simulated for the sub-glacial layer using a stochastic model based on the separation parameter (see Figure 3-8). The method chosen was stochastic, and it has allowed the simulation of networks of discrete conduits occurring in heterogeneous geological media /Jaquet et al. 2004/.

In order to avoid potentially adverse numerical effects, two conductive (deterministic) features were added along both side edges of the model. A similar definition of conductive features had been adopted in the previous glaciation modelling study /Jaquet and Siegel 2003/. Conductive features were generated for the entire model domain although, conceptually speaking, they should appear only downstream of the ELA. In effect, the small basal meltrates resulting upstream of the ELA rendered the hydraulic effect of the conductive features negligible for modelling purposes.

Finally, the hydraulic conductivity for the conductive features was calibrated such that the water pressure on average does not exceed the pressure of the ice; i.e. the lifting of the ice is avoided globally but local exceptions are permitted. A hydraulic conductivity of 2 m/s was obtained as calibrated value for the conductive features. Higher hydraulic conductivities were not considered, because such values would diminish bedrock infiltration and potentially lead to an underestimation of flow field modifications due to glaciation.

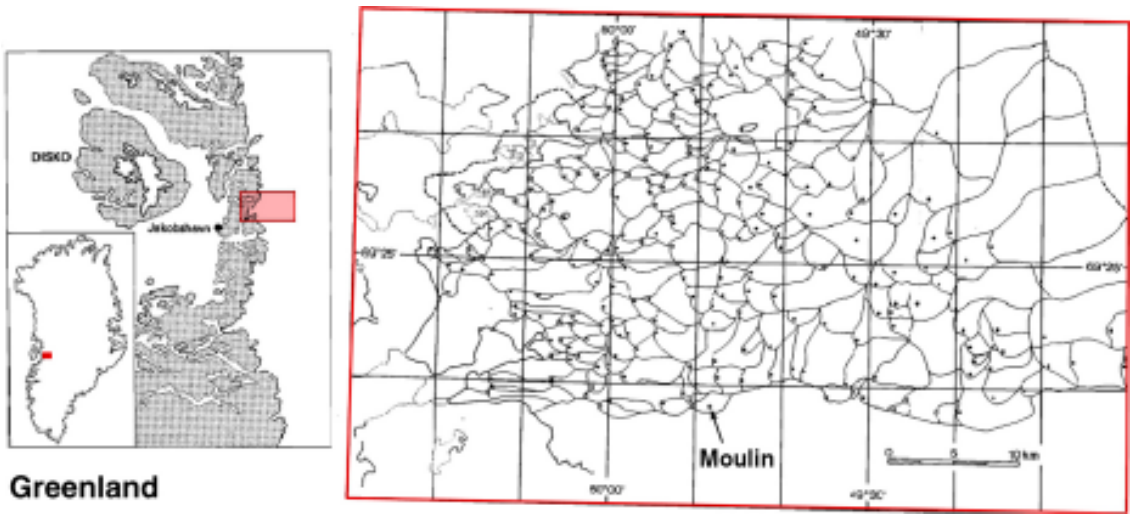

Figure 3-7. *Map of catchment areas in Greenland showing moulins on the surface of the ice sheet. The flow of ice is towards the West /After Thomsen et al. 1989/.*

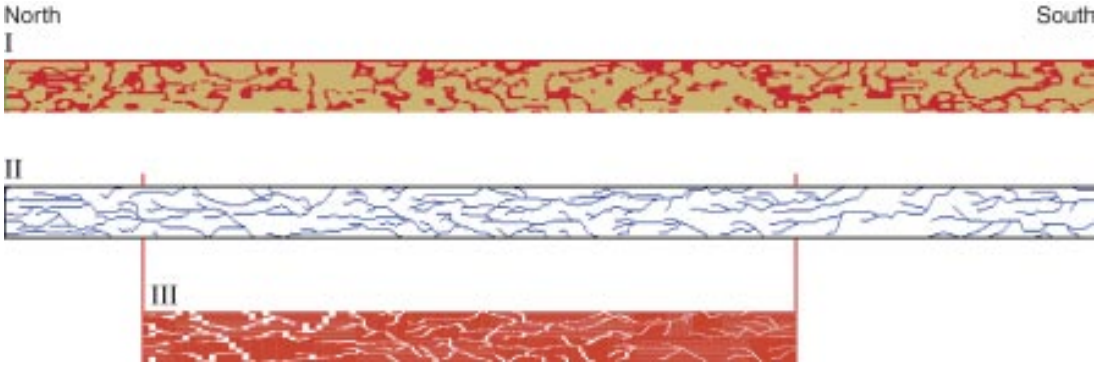

Figure 3-8. *Stochastic simulation of conductive features for the sub-glacial layer in three stages (top to bottom). Stage I: creation of the potential location of conductive features using truncated Gaussian simulations constrained with separation distance. Stage II: stochastic simulation of the geometry of conductive features conditioned with potential and ice flow direction. Stage III: downscaling of the conductive features to the glaciation model using the IFZ method /Marsic et al. 2001/.*

4 Groundwater flow modelling

Groundwater flow during a period of glaciation is modelled for the base case with the parameters defined in the preceding chapters. The initial and boundary conditions for the base case are defined below.

4.1 Initial conditions

Salinity initial conditions

For the base case, the following initial conditions for salinity are selected:

- Between ground surface and –500 m: fresh groundwater conditions.
- Between –500 m and –2,100 m: the salinity increases linearly from 0% to 10% by weight.
- Below –2,100 m: the salinity is constant at 10% by weight. This value corresponds to a density of 1,074 kg/m^3 using the relation of /Svensson 1999/: $\rho = \rho_0 (1+as)$ with the salinity, *s,* and the coefficient, *a,* equal to $7.41 \cdot 10^{-3}$.

Flow initial conditions

The initial conditions for flow were taken from a simulation performed under steady-state conditions with a fixed salt profile (cf above) in the absence of the ice sheet.

4.2 Time periods and boundary conditions

Rather than corresponding to the full period of the Weichselian glaciation, the glaciation period modelled is that relevant to the modelled domain in terms of ice being present. Within the glaciation period, the following transient effects of glaciation are considered: (a) glacial build up, (b) glacial completeness and (c) glacial retreat.

In terms of boundary conditions, the glaciation period from –30,900 to –11,400 a (expressed in years before present) is divided into five phases:

- **P0 (–30,900 a)**. Pre-glacial build up: initially, no ice sheet is present.
- **P1 (–30,900 to –25,100 a)**. Glacial build-up: the ice sheet progressively covers the model domain.
- **P2 (–25,100 to –14,100 a)**. Glacial completeness: the ice sheet covers the full domain of the model.
- **P3 (–14,100 to –11,400 a)**. Glacial retreat: the ice sheet progressively withdraws from the model domain.
- **P4 (–11,400 a)**. Post-glacial retreat: the ice sheet has completely disappeared from the model domain.

Top surface: periods P1, P2 and P3

The movement of the glacier is simulated with transient boundary conditions provided by a dynamic ice sheet model /SKB 2006/. A specific run of the ice sheet model was performed with a high spatial resolution (10×10 km) to obtain the ice thickness and the basal and surface meltwater rates needed as input for the groundwater flow model (see Figure 4-1). The ice sheet

data were available from –40,000 to –9,000 a (expressed in years before present) with a time step of 100 a /Näslund and Fastook 2005/.

All surface meltwater is assumed to reach the sub-glacial layer in the same grid cell in which it is generated. For the glaciation model the total meltrate (including basal and surface meltrate) is implemented as a prescribed transient flow boundary. On the basis of the displacement velocity of the ice sheet, the area covered by the glaciation model was divided into 16 zones of 25×25 km. For a given zone, the average (total) meltrate was estimated using the neighbouring data values provided by the ice sheet model. Cokriging /Wackernagel 2003/ was applied to estimate an average meltrate for each of the 16 zones of the glaciation model and for each time step. This procedure was selected in order to take into account the correlation between meltrate and ice thickness when estimating the flow boundary conditions using ice sheet data.

The meltrates of up to several m/a are too large to correspond physically to the groundwater recharge (Figure 4-3). Based on results from /Walker et al. 1997/, it was decided to select a maximum value of 200 mm/a for the recharge.

Atmospheric pressure is prescribed in front of the ice sheet as well as the concentration (with a value equal to zero). Also the concentration of the infiltrating glacial water is set to zero.

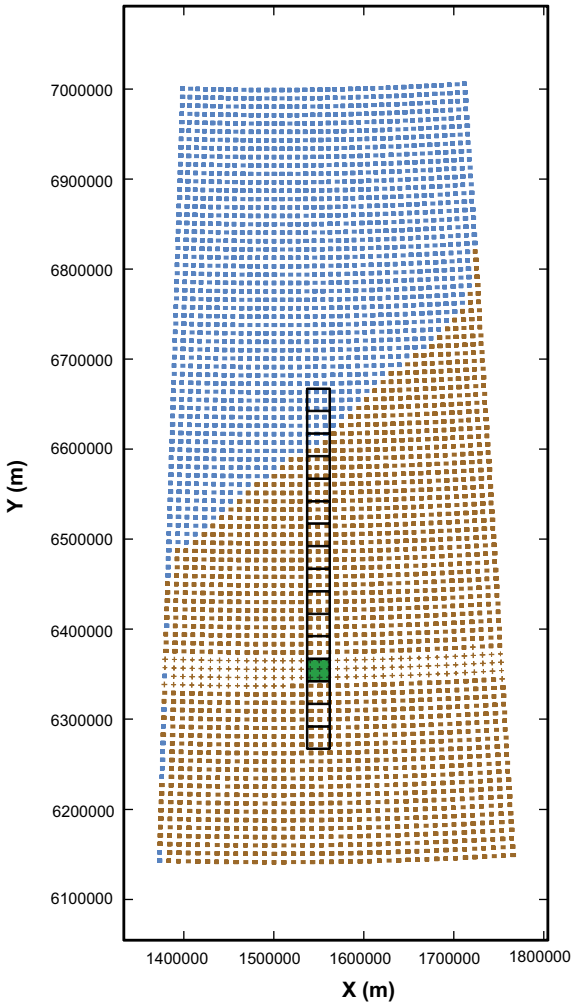

Figure 4-1. *Results of ice sheet modelling at time step –30,000 a /after Näslund and Fastook 2005/: the blue points indicating the presence of ice. Projected into the ice sheet model are the 16 zones discretised for the glaciation model to implement the ice-sheet boundary conditions. For each zone, an average meltrate was estimated by cokriging using the nearest data points. The green zone comprises the Simpevarp model area.*

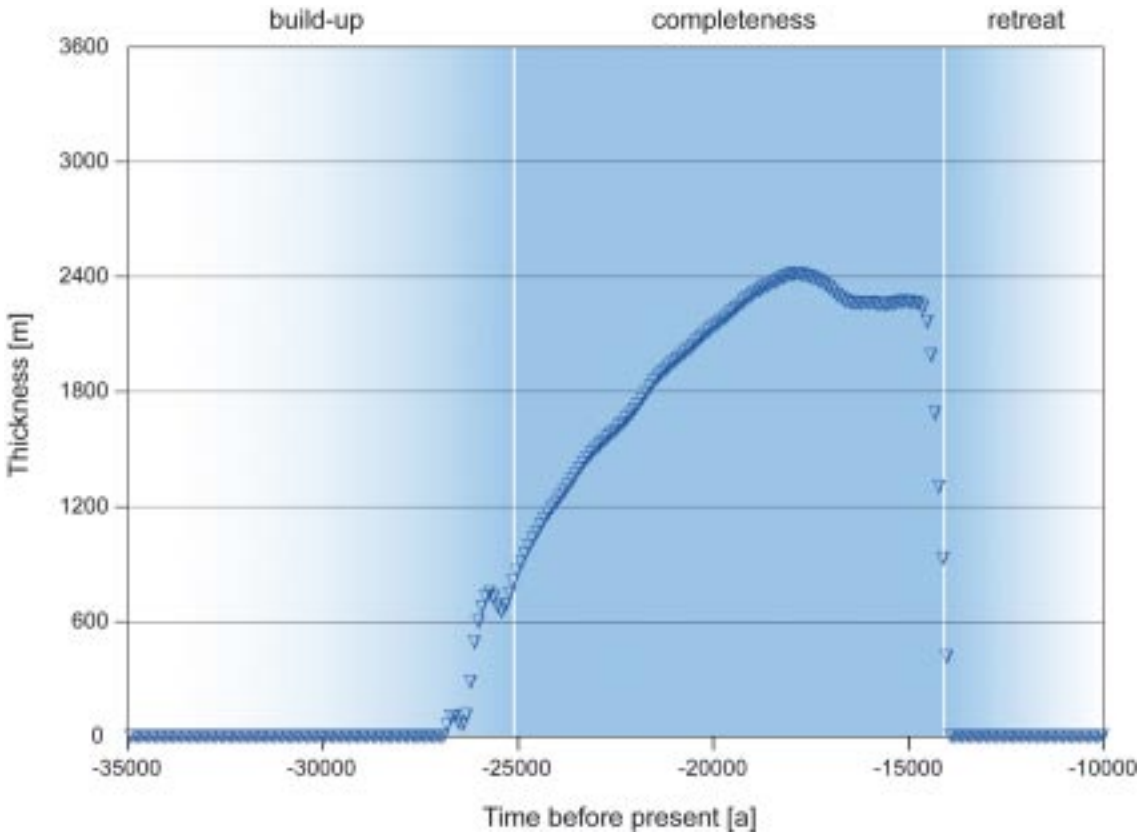

Figure 4-3. *Evolution of the total meltrate at repository location /after Näslund and Fastook 2005/.*

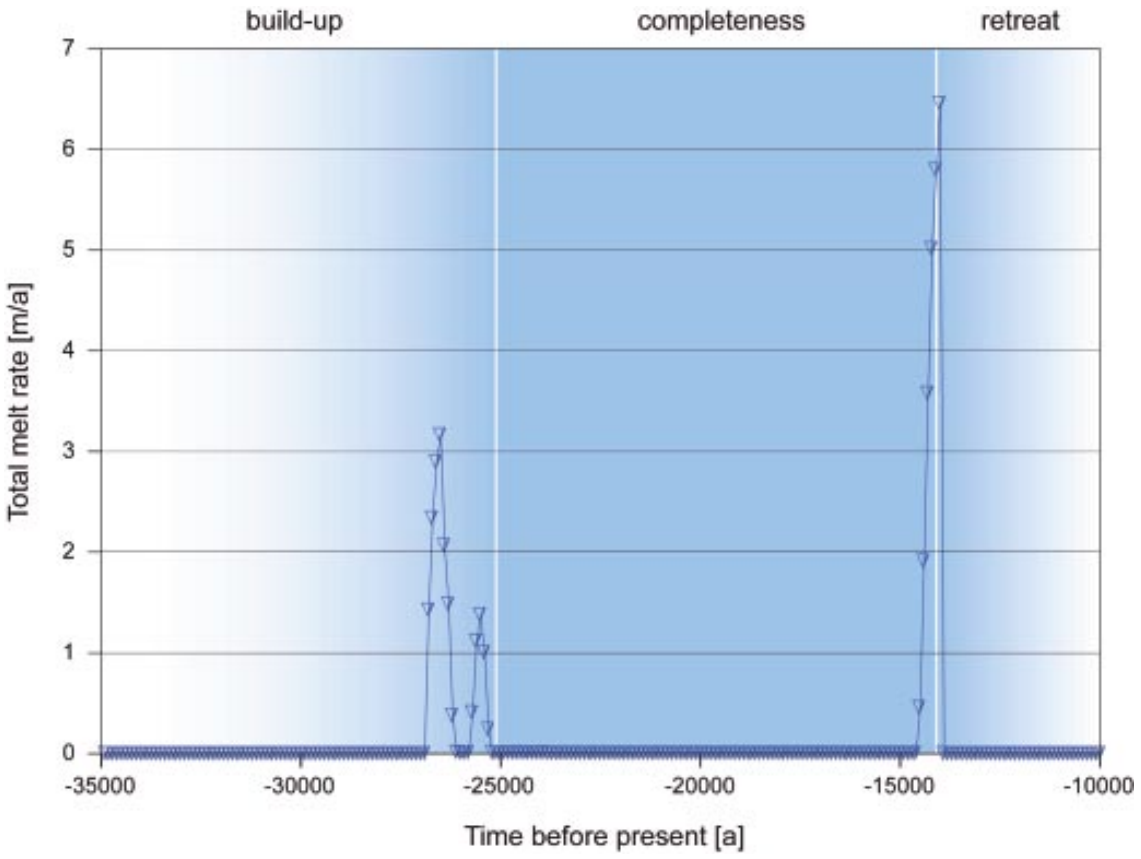

Figure 4-2. *Evolution of the thickness of the ice sheet at repository location /after Näslund and Fastook 2005/.*

Top surface: periods P0 and P4

Atmospheric pressure is prescribed everywhere as well as the concentration which is set equal to zero.

Top surface: period P2

In order to enable water to leave the model during glacial completeness, the last 5 km of the Southern top surface of the model were set to atmospheric pressure.

Bottom surface: periods P0, P1, P2, P3 and P4

The bottom surface boundary condition is taken as a no flow condition with a specified salt concentration of 10% by weight.

Lateral surfaces: periods P0, P1, P2, P3 and P4

No-flow conditions are applied on all four lateral sides.

4.3 Glaciation simulation: the base case

The glaciation simulation was performed for the base case for a period of 19,500 a (from –30,900 to –11,400 a, expressed in years before present). The following five time steps were selected as they are particularly representative of certain stages of glacial advance or retreat (see Figure 4-4):

I. Glacial build up at –26,800 a:	The front of the ice sheet meets the edge of the Simpevarp area.
II. Glacial build up at –26,500 a:	The ice sheet covers the Simpevarp area.
III. Glacial completeness at –17,900 a:	The ice sheet fully covers the glaciation-model area.
IV. Glacial retreat at –13,900 a:	The ice sheet covers the Simpevarp area.
V. Glacial retreat at –13,800 a:	The ice sheet front is located on the edge of the Simpevarp area.

An overview of the simulation results for the glaciation period (see Figure 4-5) demonstrates the glacial effects on groundwater flow for different glacial phases (5,800 a for the glacial build-up, 11,000 a for the glacial completeness and 2,700 a for the glacial retreat). The phases of build-up and retreat of the ice sheet are accompanied by large amounts of meltwater which drastically modify the flow pattern and thus strongly influence the salt concentration. In particular, up-coning effects occur at the margin of the ice sheet, i.e. due to the meltwater input that governs groundwater flow, the salinity front is moved upwards. This effect can be seen at time step 4,400 a (cf Figure 4-5).

The simulation results for the time step –26,800 a (glacial build-up), expressed in terms of relative concentration, display the striking effect of the ice sheet on the flow field (see Figure 4-6). Due to the consistent melting of the ice sheet and the heterogeneity related to the conductive features and the fractured rock domain, the concentration develops a spiky pattern. In Figure 4-6, the ice covers the upper left portion of the model illustration with the ice margin located at position ca 100,000 m along the Y axis. The horizontal cut demonstrates the marked difference between the domains on either side of the ice margin. In the area downstream of the glacier the variability of the salt concentration is mainly subjected to diffusive effects, i.e. there are no effects yet of the ice sheet.

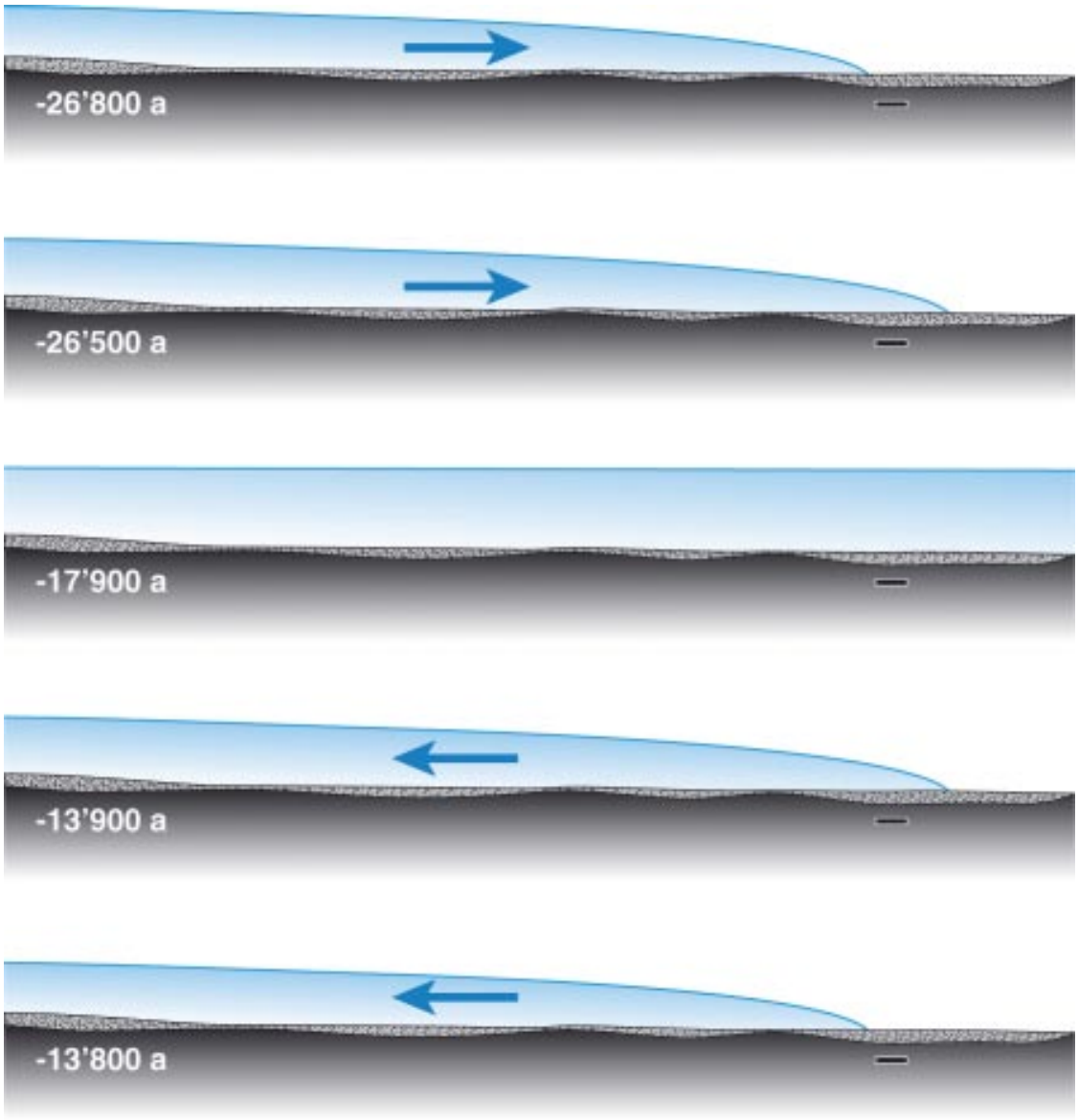

Figure 4-4. *The five selected time steps (expressed in years before present) corresponding to specific glacial conditions. The location of the Simpevarp (repository) area at depth is indicated with a black box.*

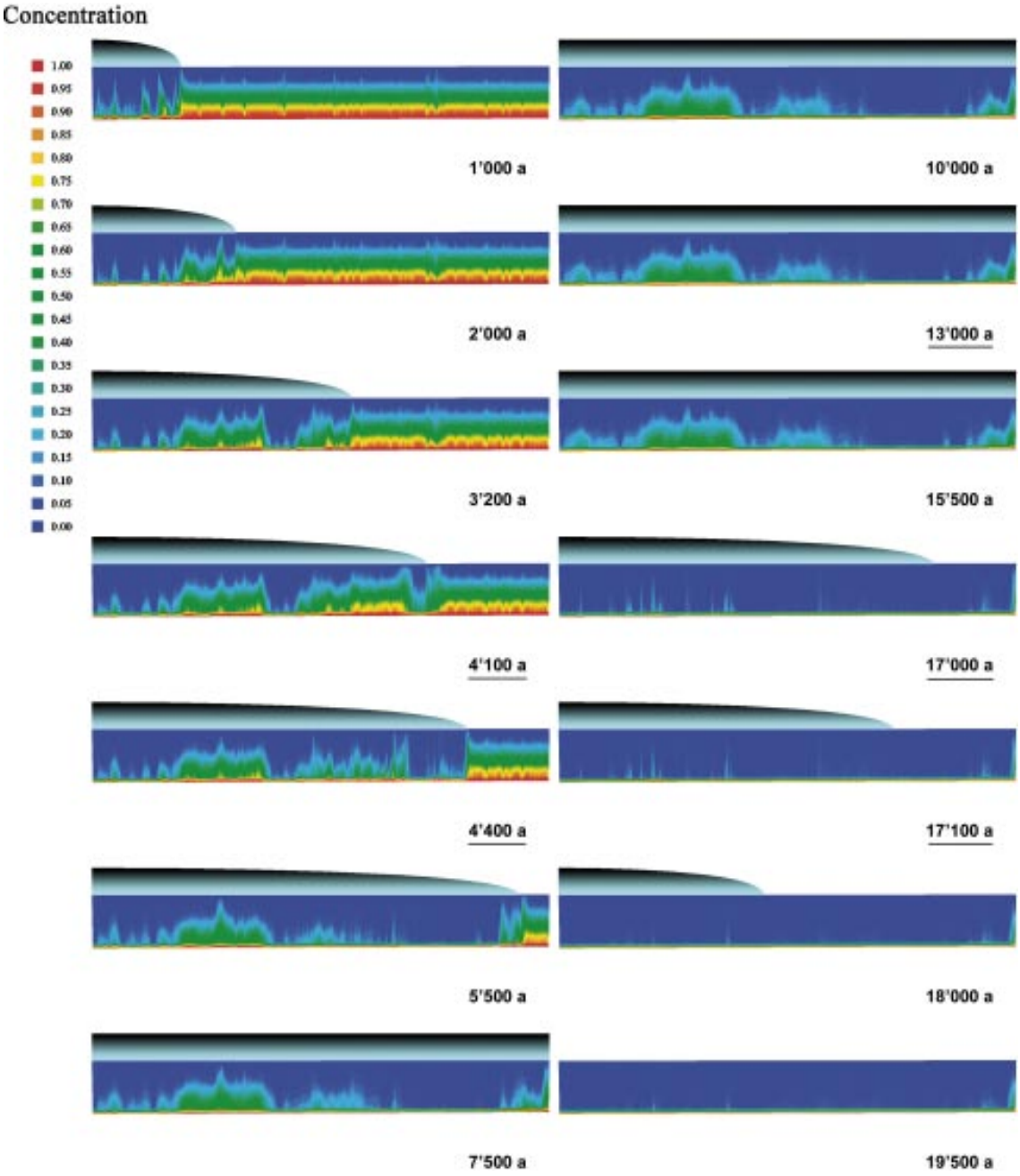

Figure 4-5. *Base case: simulation of 14 time steps, along a horizontal North – South cut (located in the middle of the model) displaying the (relative) concentration with glacial build-up (0–5,800 a), glacial completeness (5,800–16,800 a) and glacial retreat (16,800–19,500 a). The time steps are expressed in relative time (underlined values = selected time steps) and the concentration scale is identical in the following figures.*

During phases of build up and retreat, below the ice sheet, the concentration of the salt within the rock matrix is similar to the concentration with the flowing fractures (see Figure 4-6 and Figure 4-7). This observation means that the concentration of the rock-matrix and the concentration within the fractures are close to equilibrium. The high value considered for flow wetted surface (2 $m^2 \cdot m^{-3}$), enable rock-matrix diffusion to take place effectively for accessing a matrix block with a time scale of a few tens of years /Hartley et al. 2005/. In addition, the ice sheet provides large amount of meltwater with velocity likely to favour exchanges between rock matrix and fractures.

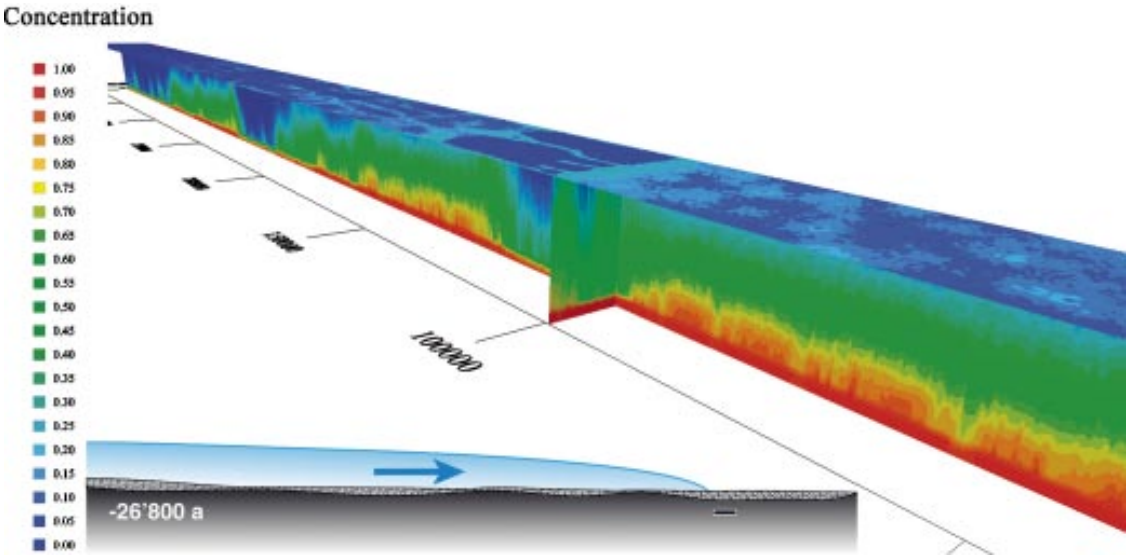

Figure 4-6. *Simulation of the base case (relative concentration) at time step –26,800 a. The ice margin is located at Y ≈ 100,000 m. The horizontal cut is at a depth of 500 m below the ground surface.*

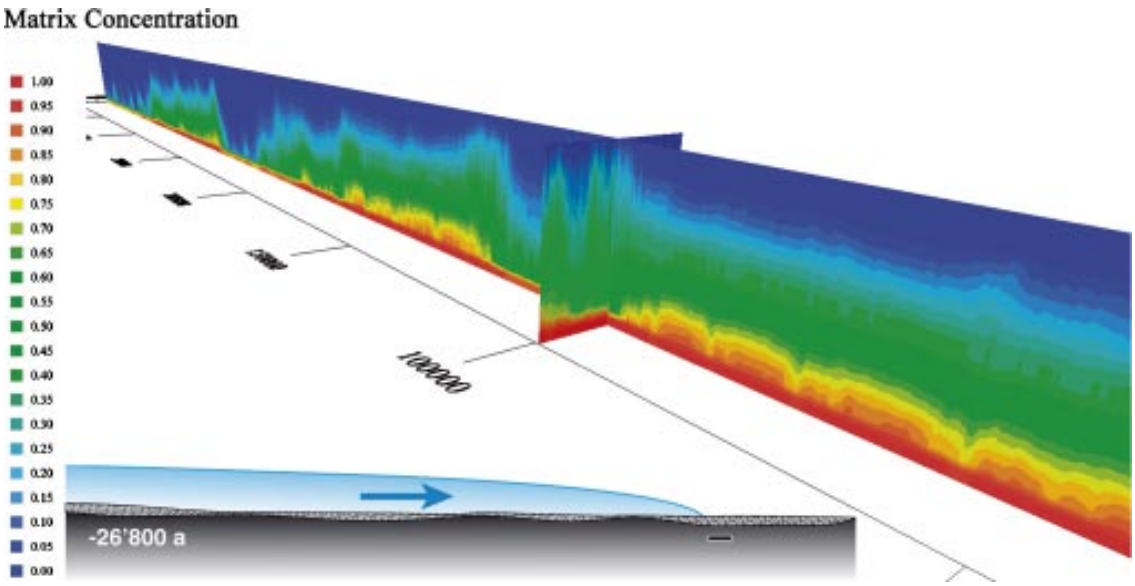

Figure 4-7. *Simulation of the base case (relative matrix concentration) at time step –26,800 a. The ice margin is located at Y ≈ 100,000 m.*

In front of the ice sheet, the concentration of the salt within the rock matrix exhibits a smoother variability than the concentration associated with the flowing fractures (see Figure 4-7). This is related to the diffusion effects occurring between the less mobile water in the rock matrix and the mobile water flowing through the fractures. Diffusion related concentration patterns tend to be more blurred than flow related concentration patterns.

The strong impact of the ice sheet on the flow field is well demonstrated by looking at the top surface of the domain at time steps –26,800 and –26,500 a (see Figure 4-8 and Figure 4-9). The high meltrate close to the ice margin leads to a substantial increase in the equivalent environmental head. The observed patterns of the head distribution are related to the space-time variations in meltrate as well as to the positions of the conductive features in the sub-glacial layer which operate as drainage structures. For the stage of glacial build-up, the attained head values are globally below the observed ice thickness (up to ca 2,800 m) which complies with the conceptual assumption (cf part 3.9).

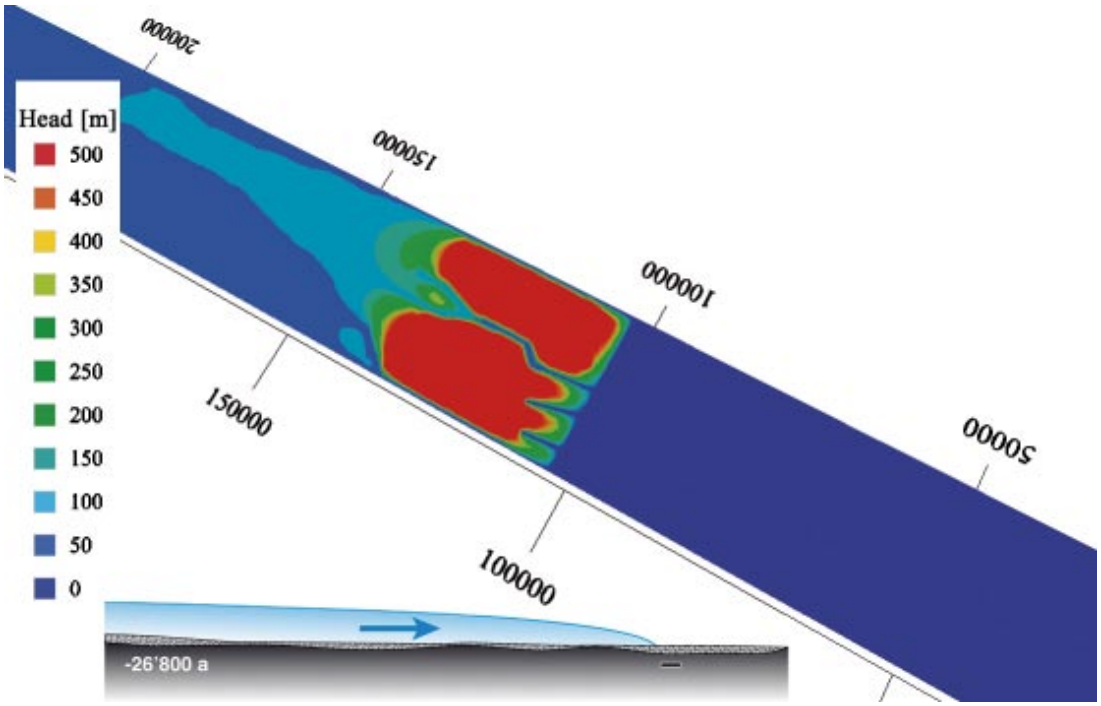

Figure 4-8. *Simulation of the base case (equivalent environmental head) at depth 0 m, for time step –26,800 a.*

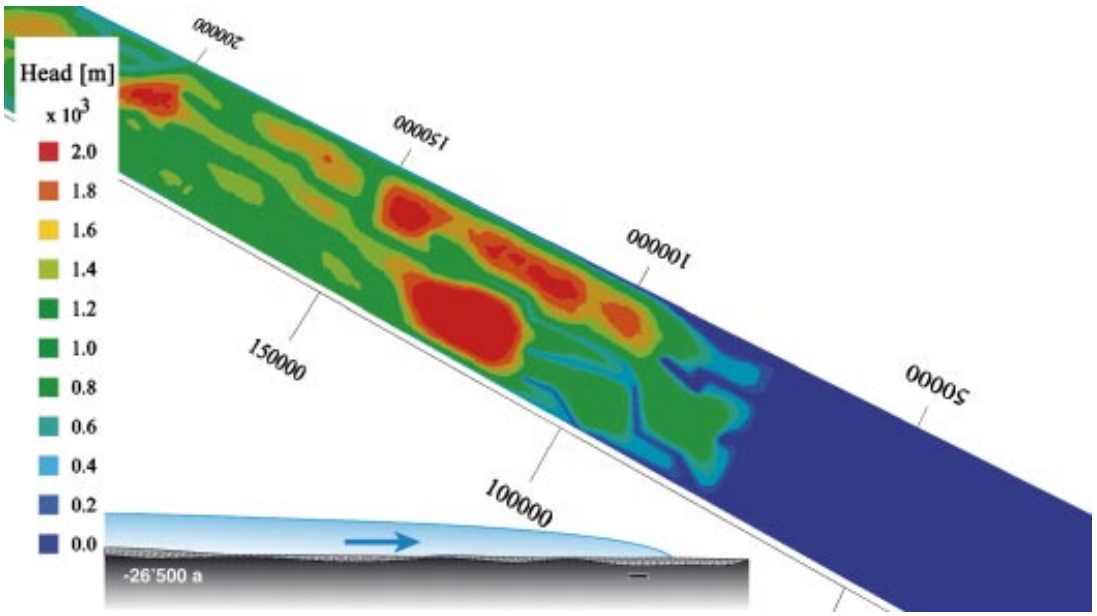

Figure 4-9. *Simulation of the base case (equivalent environmental head) at depth 0 m, for time step –26,500 a.*

During the advance of the ice sheet, more meltwater is introduced to the model. As a consequence, the flushing front (located at the ice margin) progresses with the ice sheet as it grows towards the South (see Figure 4-10). The salt concentration within the matrix follows a similar pattern as the flowing concentration as the ice sheet advances (see Figure 4-11). For this time step (–26,500 a), remarkable up-coning effects can be observed at the ice margin.

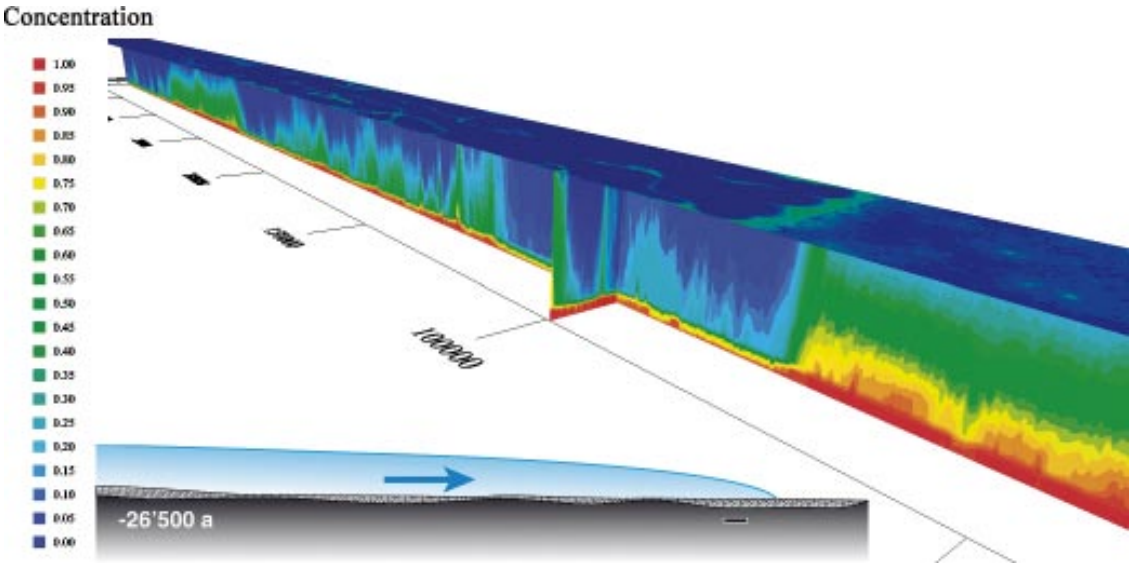

Figure 4-10. *Simulation of the base case (relative concentration) at time step –26,500 a. The ice margin south of the Simpevarp area. The horizontal cut is at a depth of 500 m below the ground surface.*

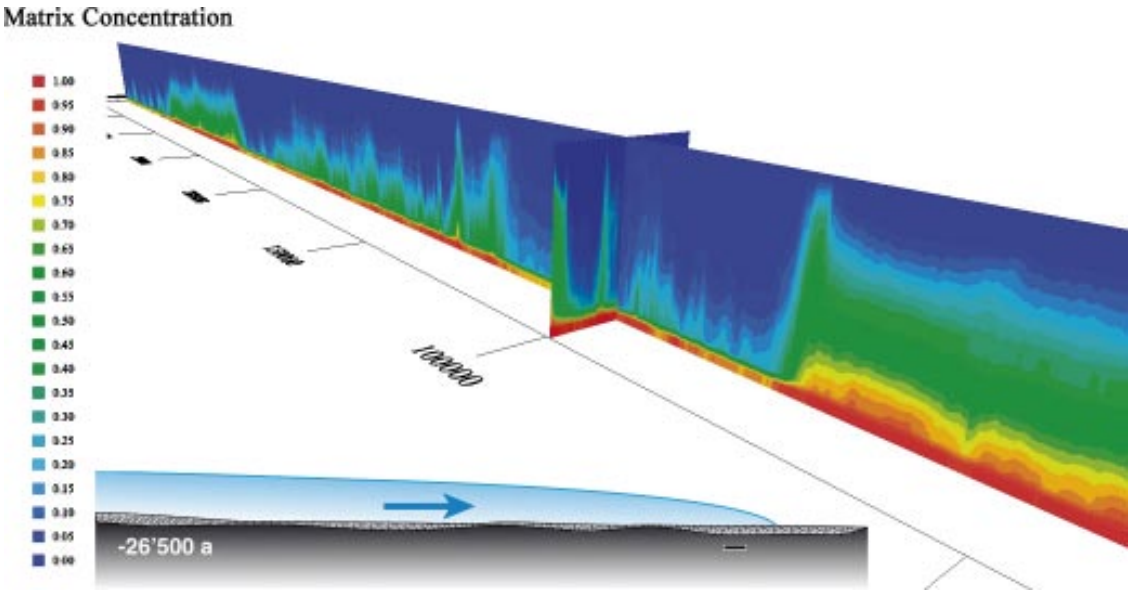

Figure 4-11. *Simulation of the base case (relative matrix concentration) at time step –26,500 a. The ice margin is located south of the Simpevarp area.*

During glacial completeness, the rate of meltwater production reaches low values as the ice sheet is not displaced. This situation leads to a stabilisation of the concentration patterns in the flow field (see Figure 4-12 and Figure 4-13 as well as Figure 4-5).

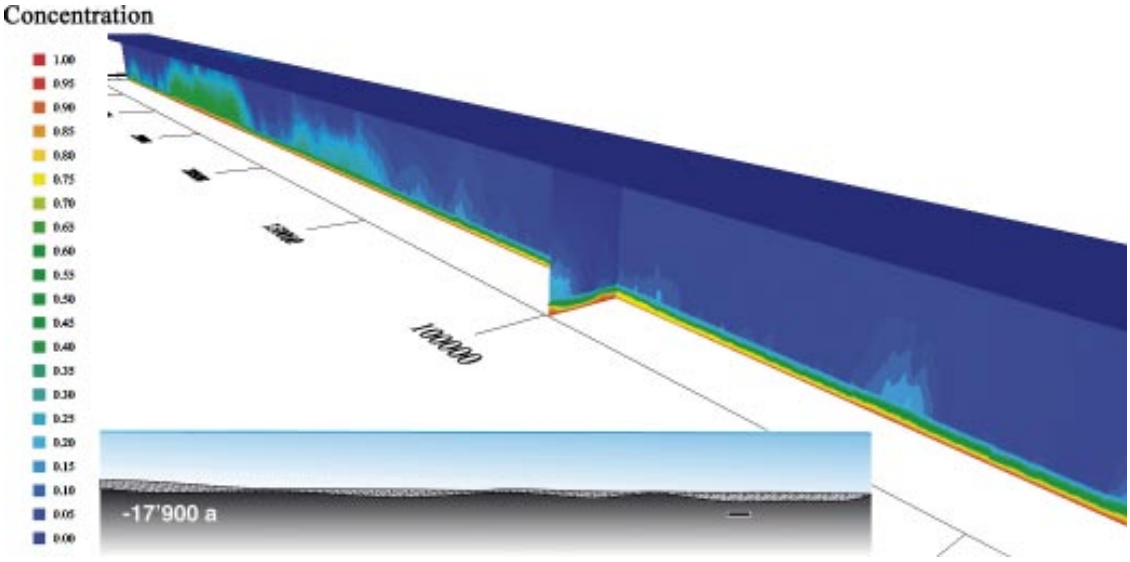

Figure 4-12. *Simulation of the base case (relative concentration) at time step –17,900 a. The horizontal cut is at a depth of 500 m below the ground surface.*

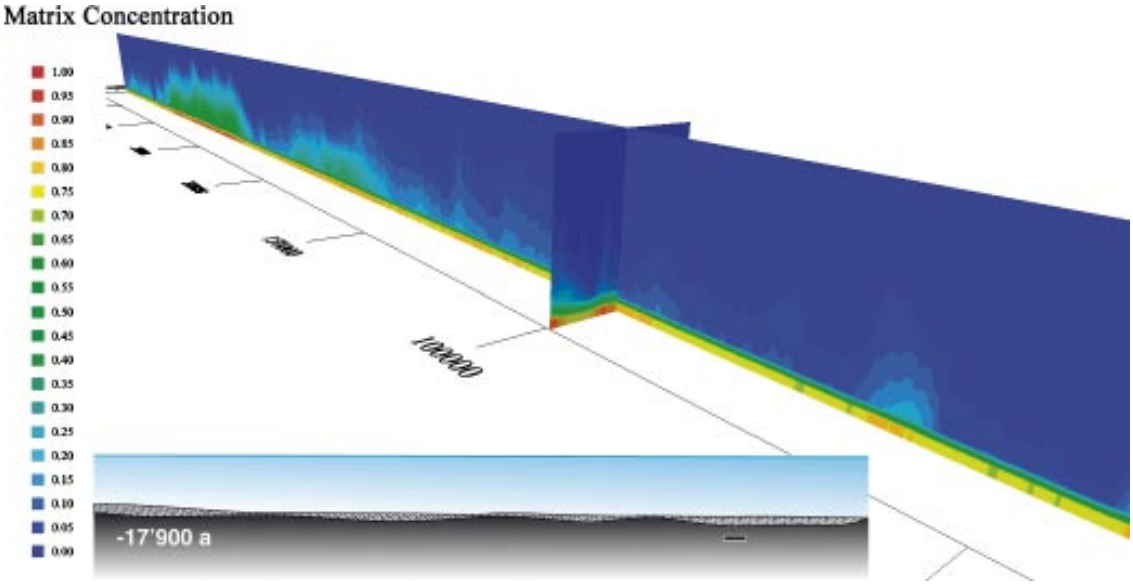

Figure 4-13. *Simulation of the base case (relative matrix concentration) at time step –17,900 a.*

During glacial retreat around ca –14,000 a, the amount of meltwater increases significantly; at the scale of almost the entire glaciation domain, the rate of meltwater recharge reaches the maximum value of 200 mm/a for a short period of time. As a consequence, due to this strong freshwater contribution from the ice sheet, the concentration fields are almost completely flushed up to the top of the bottom layer (with low hydraulic conductivity) located below 2,100 m (see Figure 4-14 and Figure 4-15).

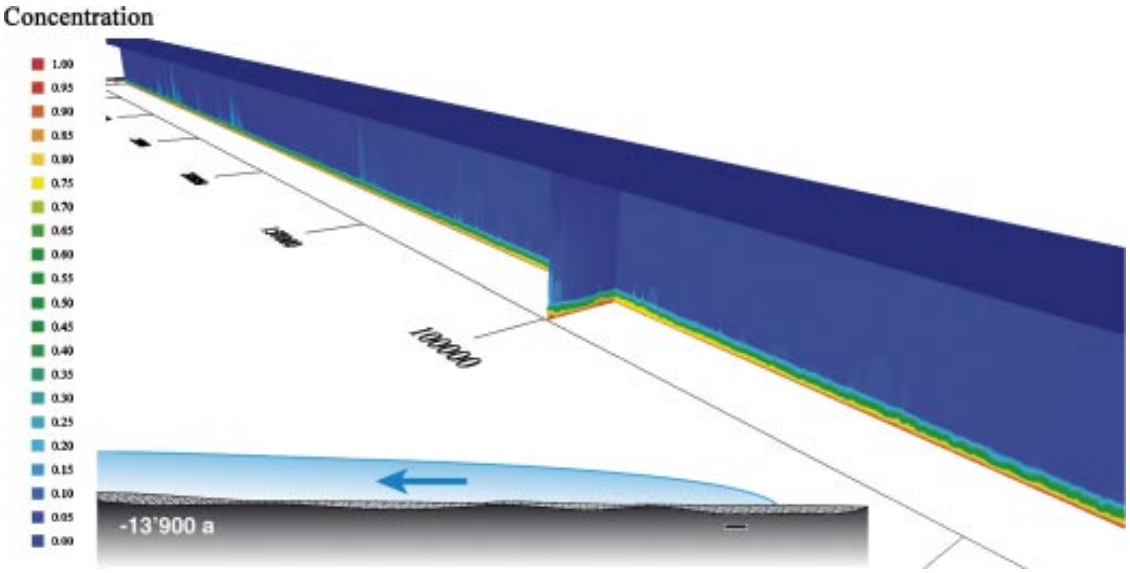

Figure 4-14. *Simulation of the base case (relative concentration) at time step –13,900 a. The ice margin is located south of the Simpevarp area. The horizontal cut is at a depth of 500 m below the ground surface.*

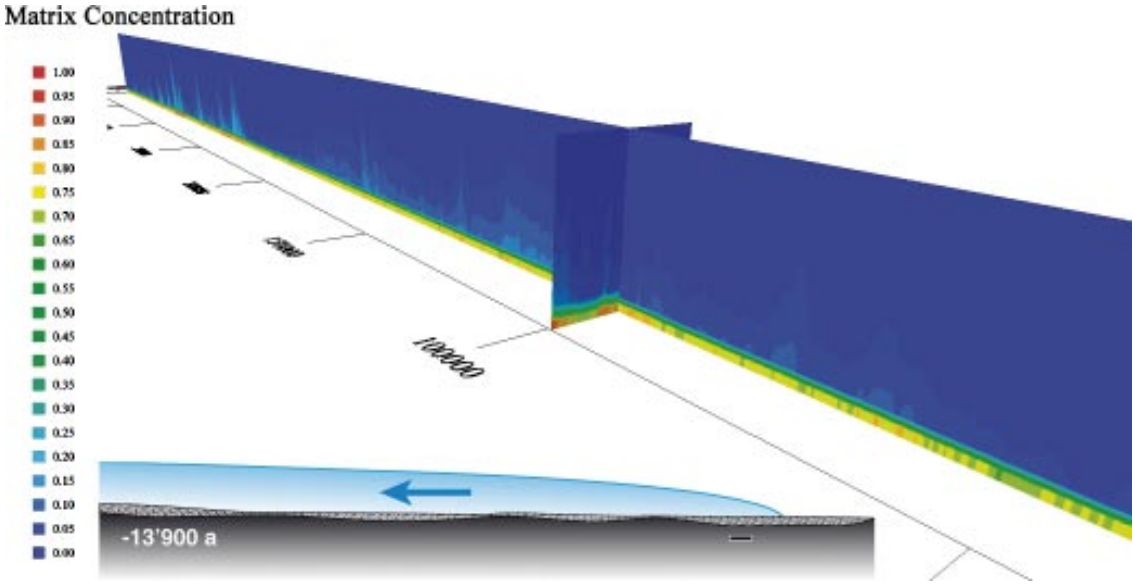

Figure 4-15. *Simulation of the base case (relative matrix concentration) at time step –13,900 a. The ice margin is located south of the Simpevarp area.*

For the stage of glacial retreat, some of the attained head values are above the observed ice thickness (up to ca 2,800 m: see Figure 4-16 and Figure 4-17). Due to the high rate of meltwater recharge, calibration of the hydraulic conductivity for the ice features could not be achieved using realistic values.

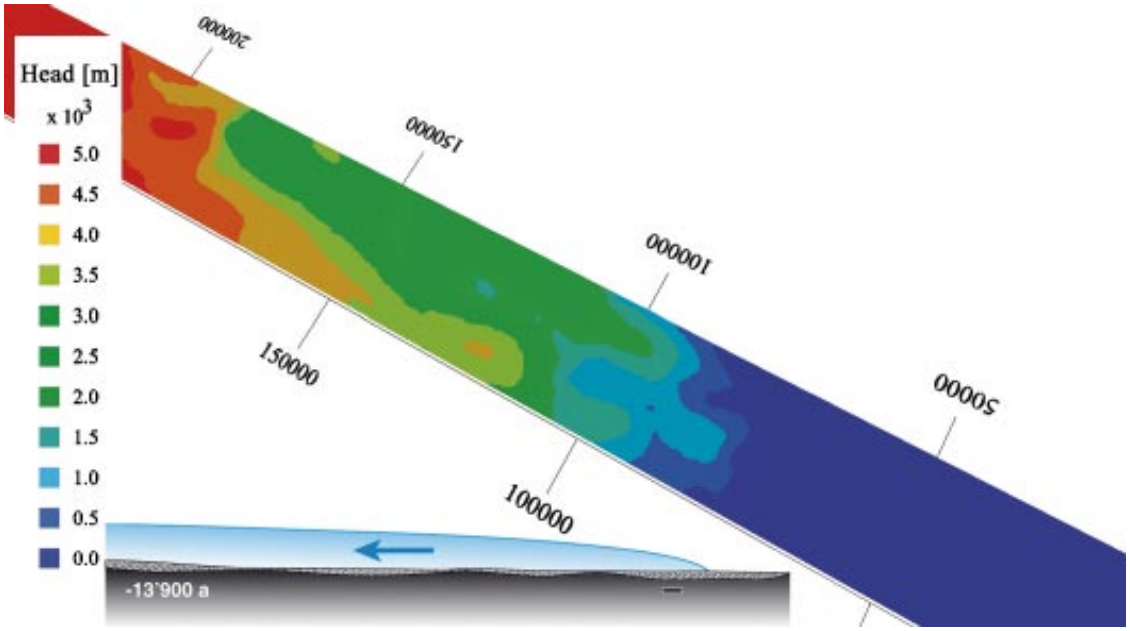

Figure 4-16. *Simulation of the base case (equivalent environmental head) at depth 0 m, for time step –13,900 a.*

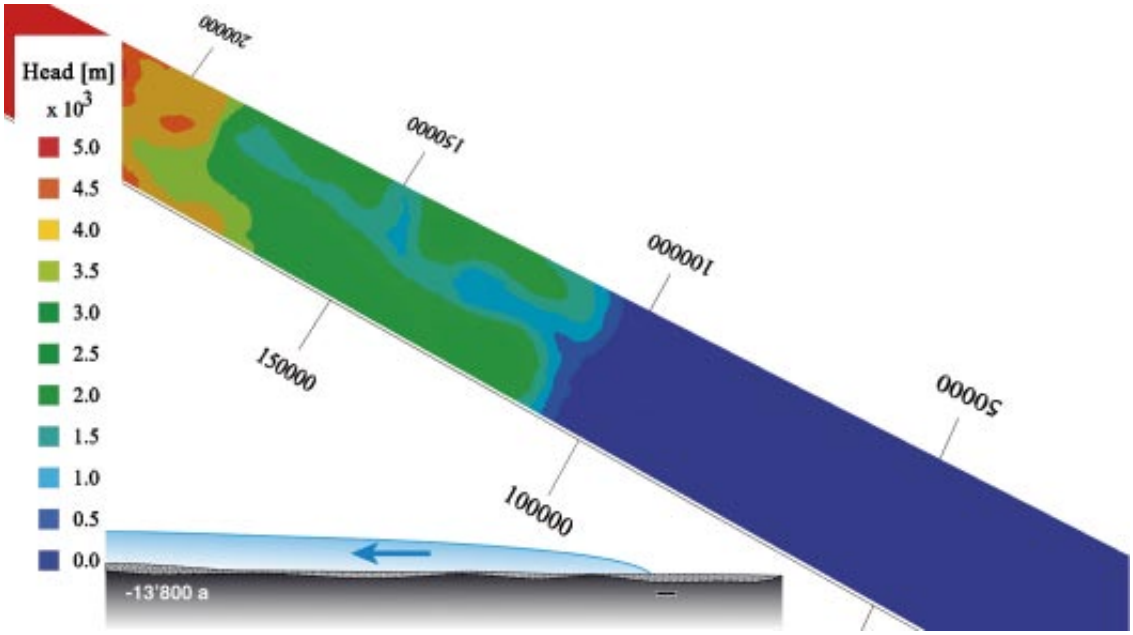

Figure 4-17. *Simulation of the base case (equivalent environmental head) at depth 0 m, for time step –13,800 a.*

As the retreat of the ice sheet continues, some meltwater is still produced, leading to an almost uniform concentration field at the end of the simulation at time step –11,400 a (see Figure 4-18, Figure 4-19 and Figure 4-5).

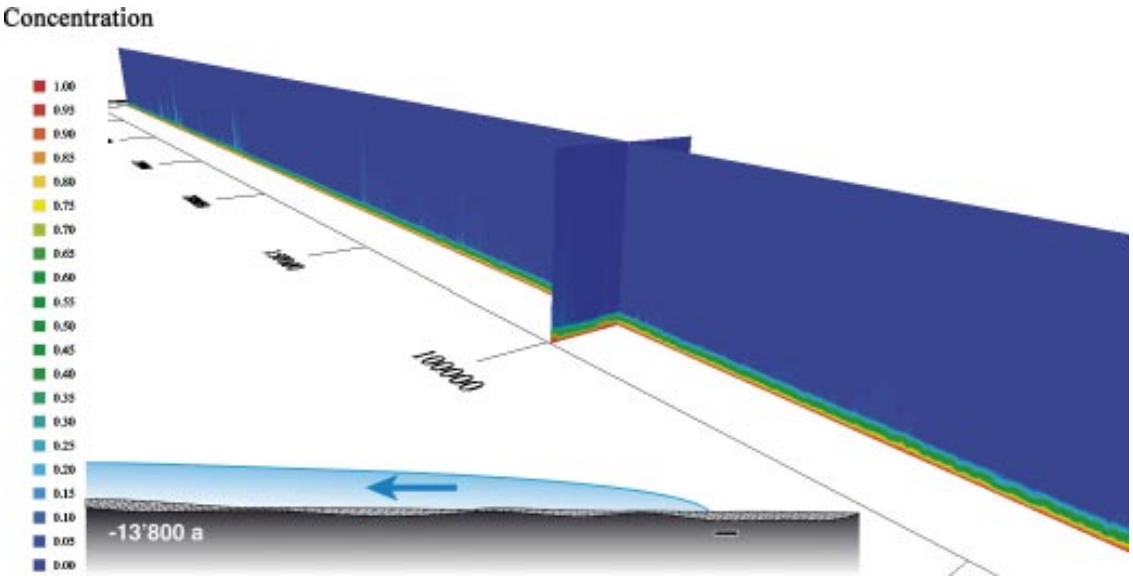

Figure 4-18. *Simulation of the base case (relative concentration) for time step –13,800 a. The ice margin is located at Y ≈ 100,000 m.*

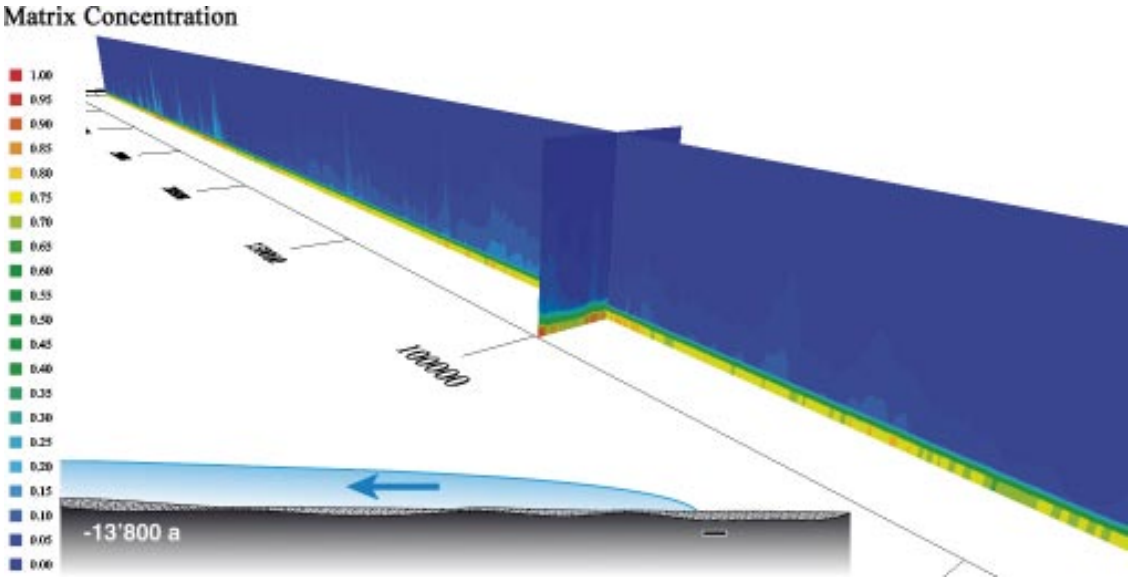

Figure 4-19. *Simulation of the base case (relative matrix concentration) for the time step –13,800 a. The ice margin is located at Y ≈ 100,000 m.*

The evolution of the flow patterns was analysed at the repository location at a depth of 500 m. The arrival and the retreat of the ice sheet at Simpevarp leads to a strong increase in the Darcy velocity due to high rates of meltwater recharge (cf the velocity peaks of Figure 4-20). The thickness of the ice sheet grows progressively during the phases of glacial build-up and glacial completeness. However, the phase of glacial retreat sees the ice sheet disappear within a few centuries (cf Figure 4-2).

Remembering the initial salinity profile, at time step –30,900 a, the concentration at 500 m is zero (cf part 4.1 salinity initial condition). The phase of glacial build-up starts with an increase in the fracture and matrix concentration mainly because of diffusive effects. The up-coning effects described above (cf Figure 4-5, Figure 4-10 and Figure 4-11) could not be captured at the repository scale due to the spatial discretisation of the ice sheet displacement. That is to say, the ice sheet progresses in steps of 25 km and the repository is located between two subsequent positions of the ice margin. As a result, up-coning effects occurring upstream and downstream of the repository remain imperceptible.

A soon as the ice sheet approaches the Simpevarp area, around –26,800 a, the concentration profiles undergo a steep decrease related to the advection of large amounts of meltwater produced by the ice sheet. Then, during glacial completeness and glacial retreat no more variability is observed in concentration, since most of the salinity was flushed out by the meltwater. The concentration values remain low until the end of the simulation.

As mentioned earlier, similar concentration changes are observed in the flowing fractures and in the matrix. The calculation of the characteristic diffusion time $\varphi_m/4\ D_{int}\ \zeta^2$; after /Hoch and Jackson 2004/ gives a value of ca 20 a. This corresponds to a time estimate for the salinity to diffuse into the rock matrix. At the scale of the time step considered for the simulation, the salinity is capable of accessing most of the rock matrix. Therefore, differences in concentration between flowing fractures and the rock matrix are less likely to occur when comparing selected time step.

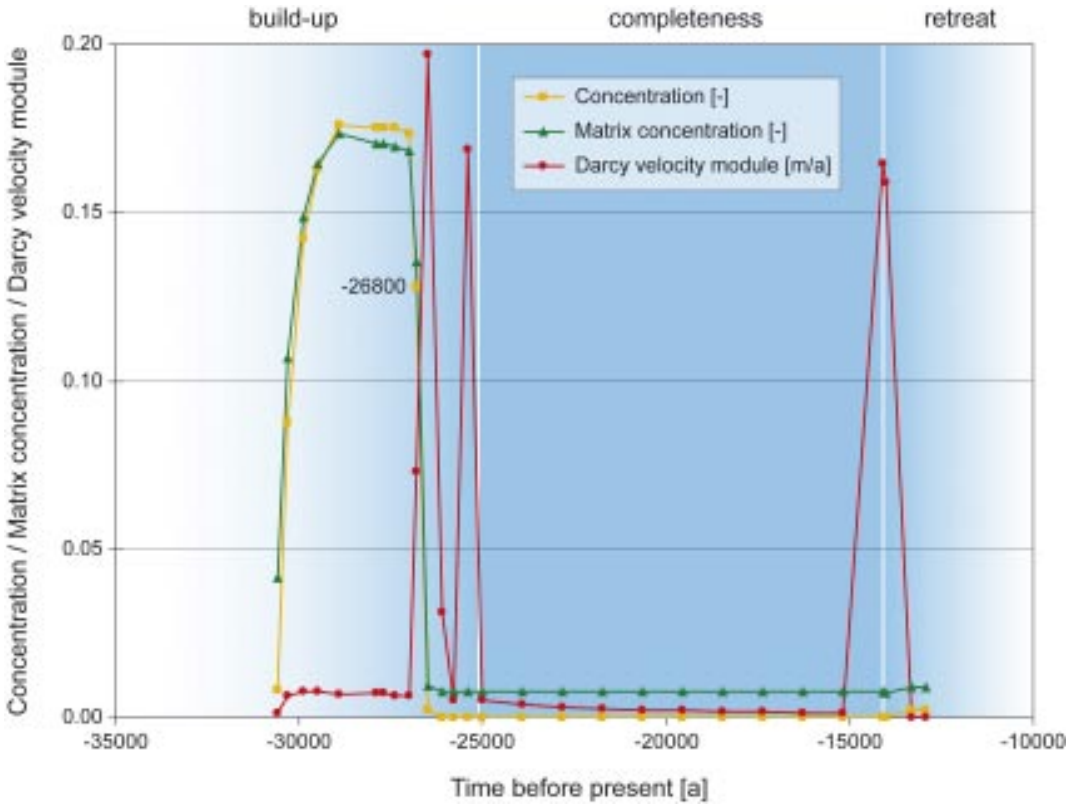

Figure 4-20. *Base case: evolution of (relative) concentration and Darcy velocity module (expressed in m/a) at repository location (500 m depth) during glacial phases.*

4.4 Glaciation simulation: 50 mm case

For the 50 mm case, the glaciation simulation was performed with a maximum meltwater recharge equal to 50 mm/a. This sensitivity case aims at evaluating the effects of one of the most uncertain parameters of the model (recalling that the maximum recharge for the base case value was set to 200 mm/a). The value chosen for the maximum recharge corresponds to the constant value used for the previous glaciation model /Jaquet and Siegel 2003/. For comparison purposes, the results of the 50 mm case were produced at the same time steps as those for the base case (– 26,800 a, –26,500 a, –17,900 a, –13,900 a and –13,800 a).

For the time step –26,800 a (glacial build up), the effects of the meltwater on the flow field are still considerable; however, in comparison to the base case, the depth of penetration of the meltwater for the 50 mm case seems less pronounced in some parts of the model (see Figure 4-21 and Figure 4-22).

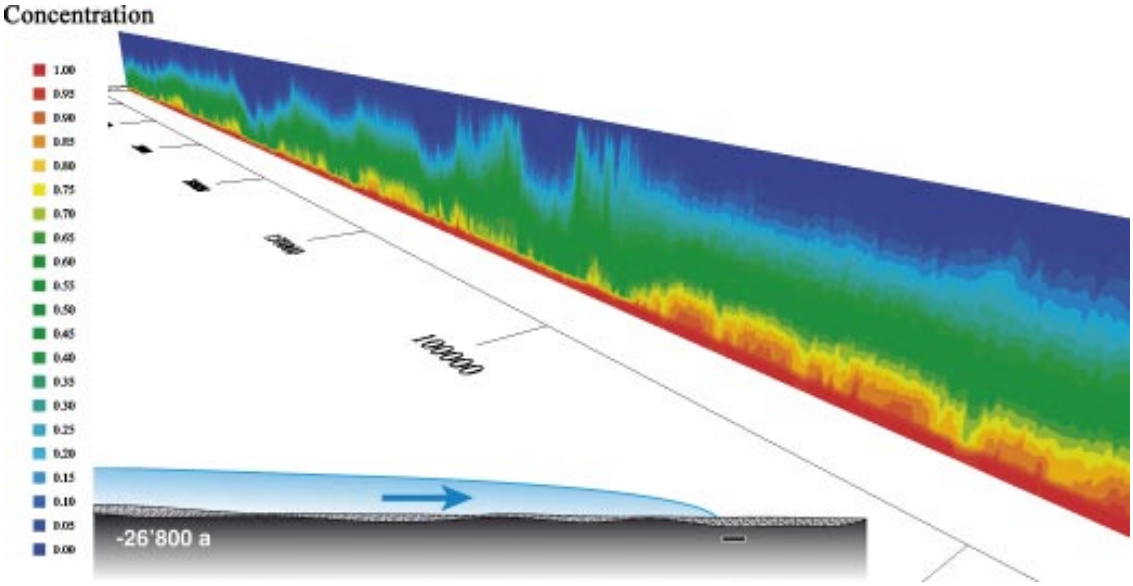

Figure 4-21. *Simulation of the 50 mm case (relative concentration) at time step –26,800 a. The ice margin is located at Y ≈ 100,000 m.*

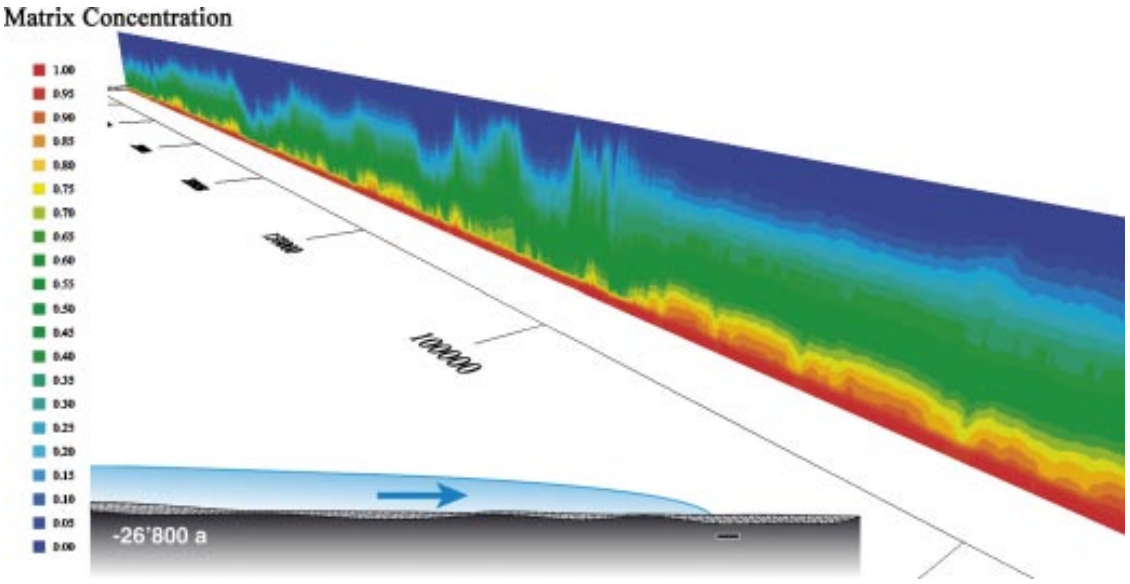

Figure 4-22. *Simulation of the 50 mm case (relative matrix concentration) at time step –26,800 a. The ice margin is located at Y ≈ 100,000 m.*

In front of the ice sheet, diffusion effects – similar to the base case – are observed. In particular, diffusion-related concentration patterns tend to be smoother than flow-related concentration patterns (see Figure 4-22).

During glacial build-up, increasing amounts of meltwater are introduced to the model as the ice sheet progresses. The overall consequences for the flow field are similar to the base case; however, the depth of penetration for the meltwater decreases in comparison to the base case, especially when getting closer to the ice margin (see Figure 4-23). The salt concentration within the matrix follows a similar pattern as the flowing concentration during this glacial phase (see Figure 4-24). Like for the base case, up-coning effects can be observed at the ice margin.

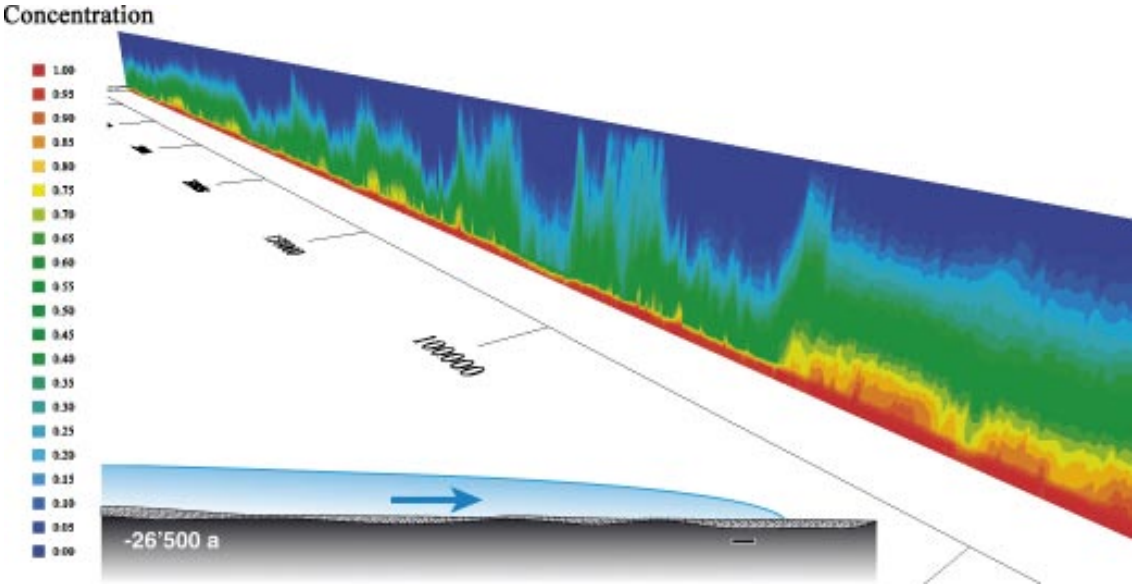

Figure 4-23. *Simulation of the 50 mm case (relative concentration) at time step –26,500 a. The ice margin is located south of the Simpevarp area.*

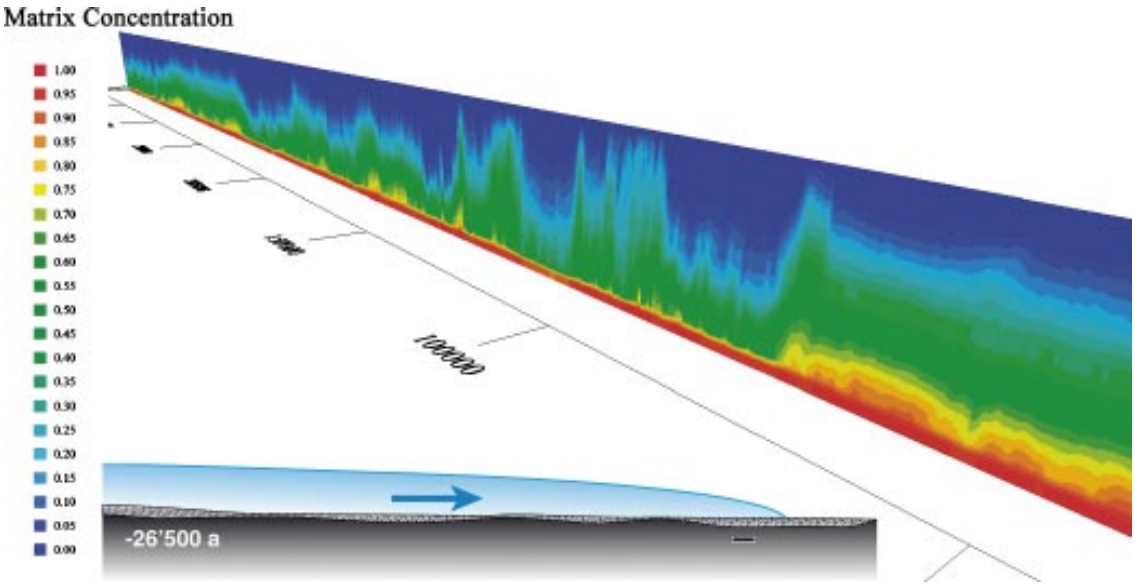

Figure 4-24. *Simulation of the 50 mm case (relative matrix concentration) at time step –26,500 a. The ice margin is located of the Simpevarp area.*

During glacial completeness, the rate of meltwater recharge decreases as the ice sheet does not move. Compared to the base case, there is more salinity in the model, since less meltwater was produced during the build-up phase; i.e. this case being characterised by a maximum recharge of 50 mm/a (see Figure 4-25 and Figure 4-26).

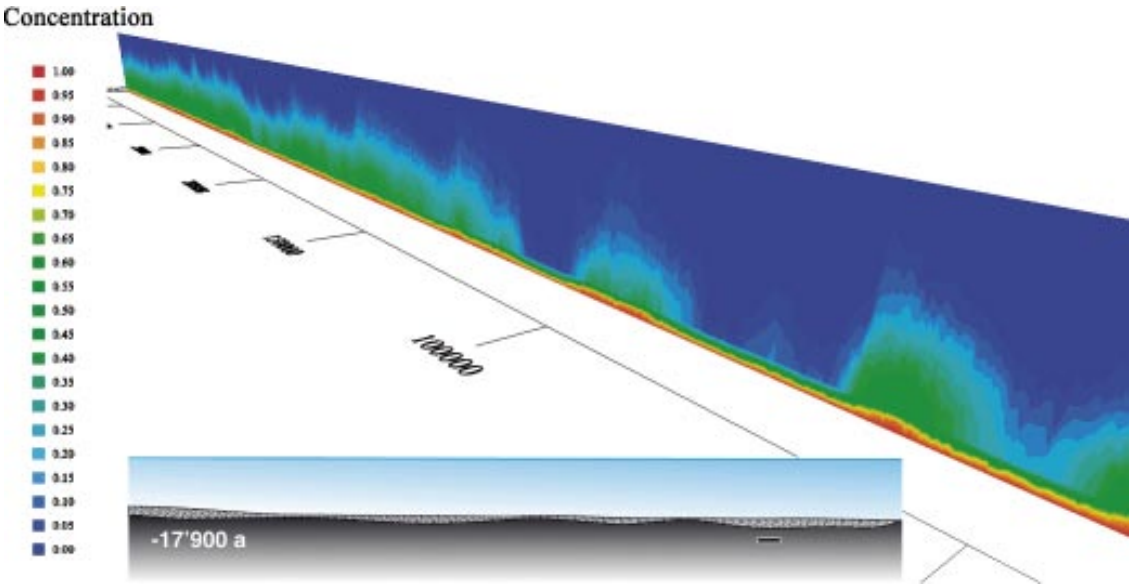

Figure 4-25. *Simulation of the 50 mm case (relative concentration) at time step –17,900 a. The ice margin is located at Y ≈ 100,000 m.*

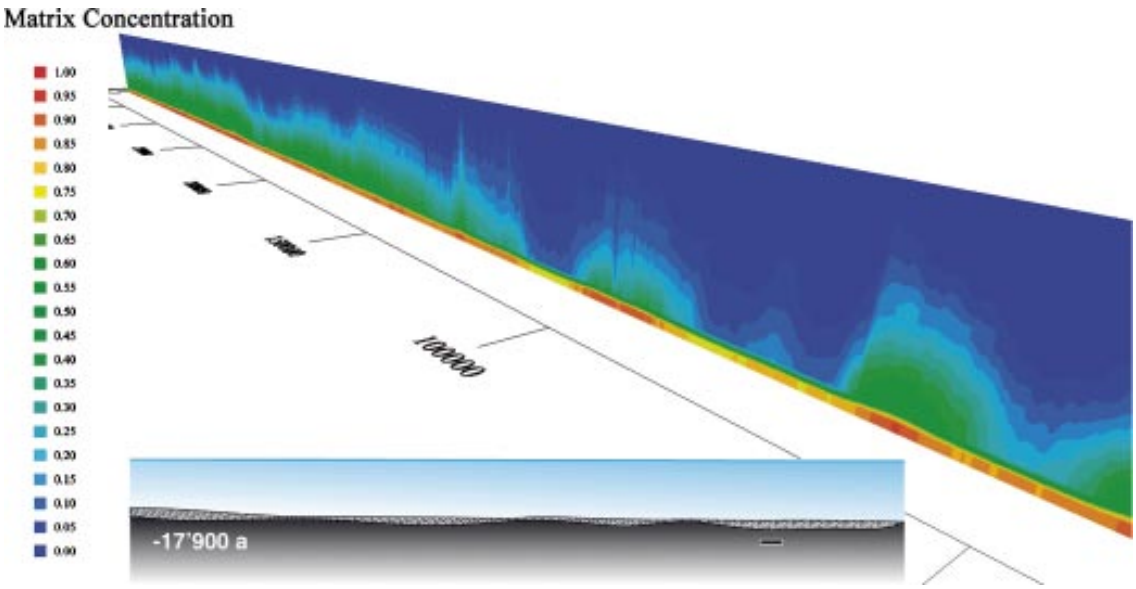

Figure 4-26. *Simulation of the 50 mm case (relative matrix concentration) at time step –17,900 a.*

During glacial retreat (around ca –14,000 a), the meltwater rate reaches the maximum value of 50 mm/a for a short period of time at the scale of almost the entire model domain. For this case, the flushing with meltwater is still important but to a lesser extent than for the base case; some salinity remains within the model domain (see Figure 4-27 and Figure 4-28).

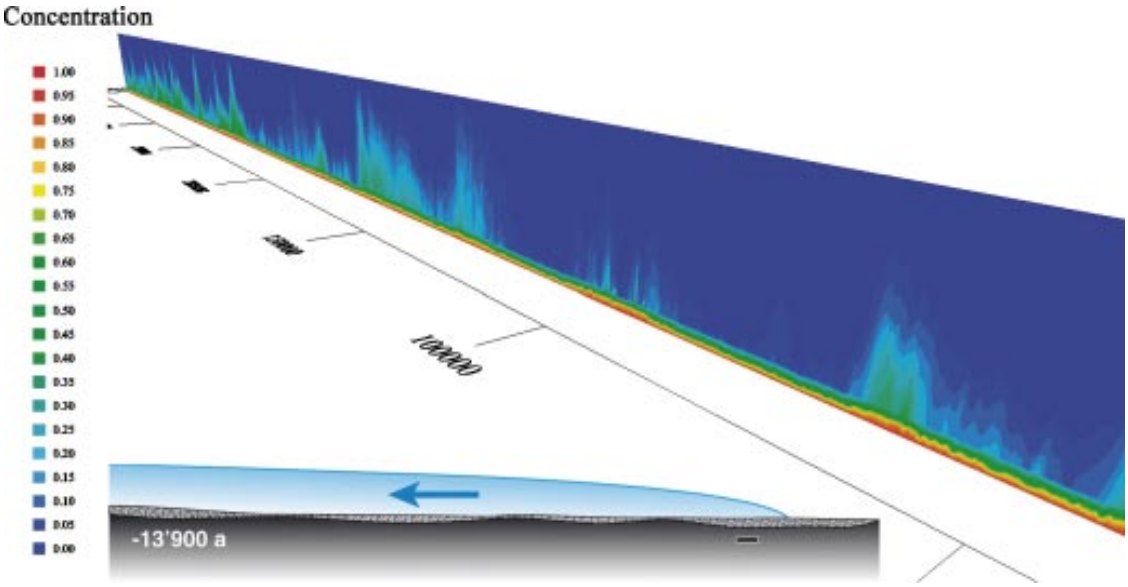

Figure 4-27. *Simulation of the 50 mm case (relative concentration) at time step –13,900 a. The ice margin is located south of the Simpevarp area.*

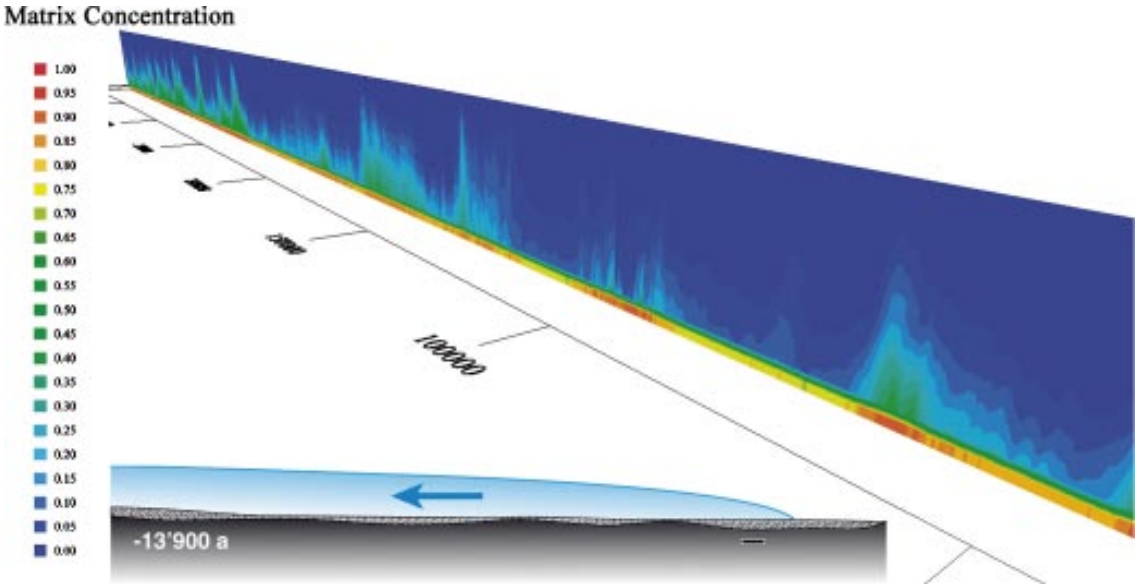

Figure 4-28. *Simulation of the 50 mm case (relative matrix concentration) at time step -13,900 a. The ice margin is located south of the Simpevarp area.*

For the 50 mm case, the attained head values are well below the observed ice thickness (up to ca 2,800 m) for the stages of glacial retreat (see Figure 4-29 and Figure 4-30).

As the glacial retreat continues, the meltwater produced no longer modifies the concentration patterns of the flow field; i.e. at –13,800 a, the resulting concentration field is similar to that of the previous time step (see Figure 4-31 and Figure 4-32).

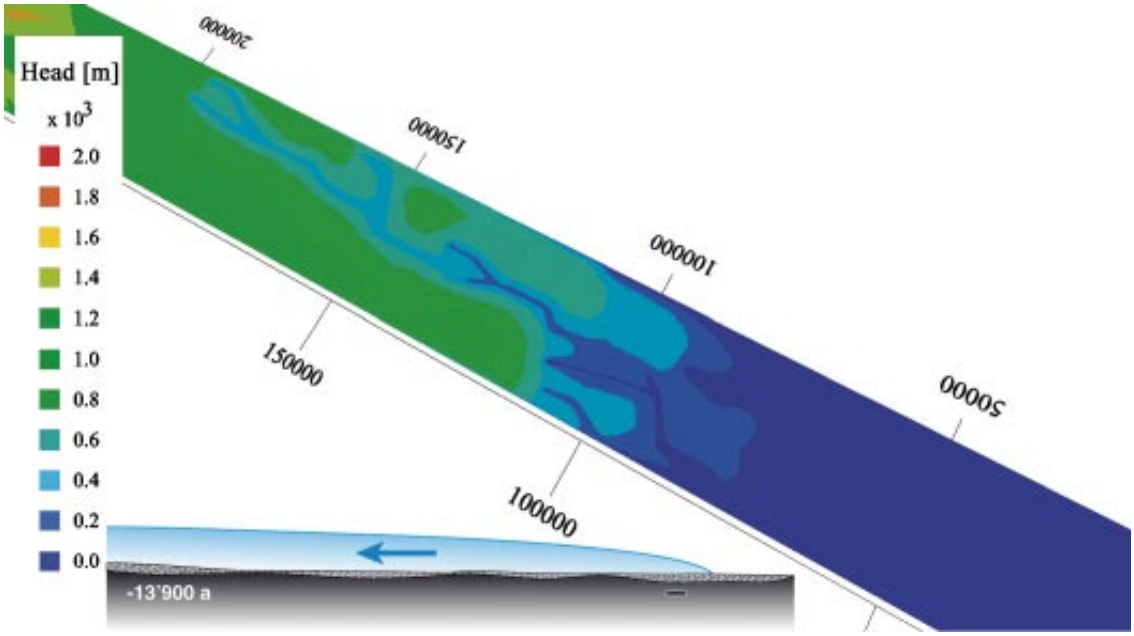

Figure 4-29. *Simulation of the 50 mm case (equivalent environmental head) at depth 0 m, for time step –13,900 a.*

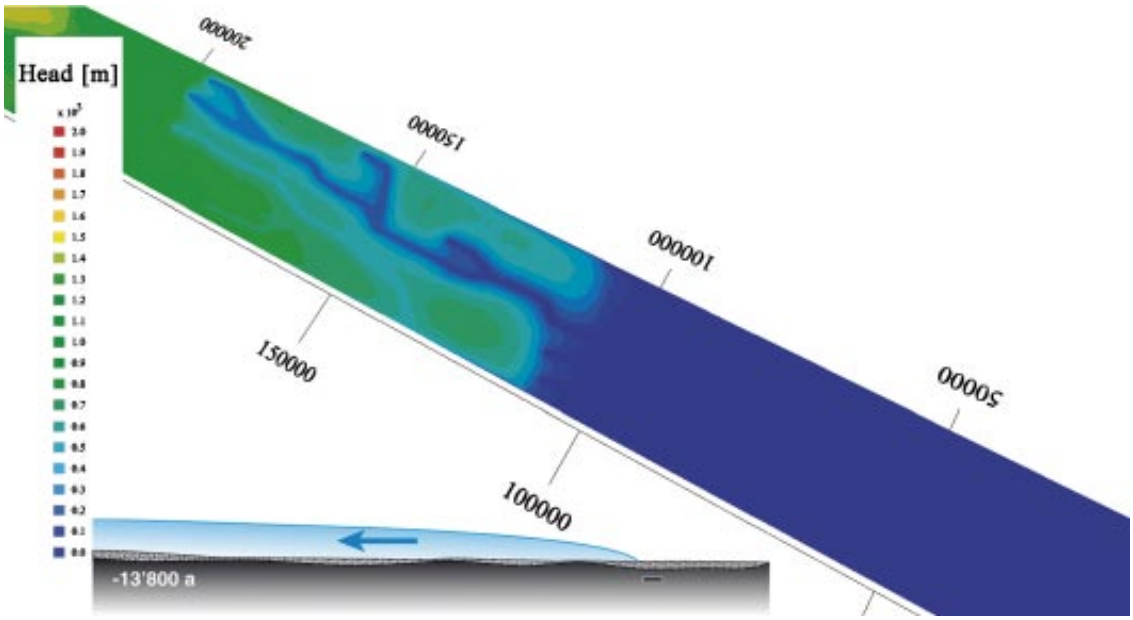

Figure 4-30. *Simulation of the 50 mm case (equivalent environmental head) at depth 0 m, for time step –13,800 a.*

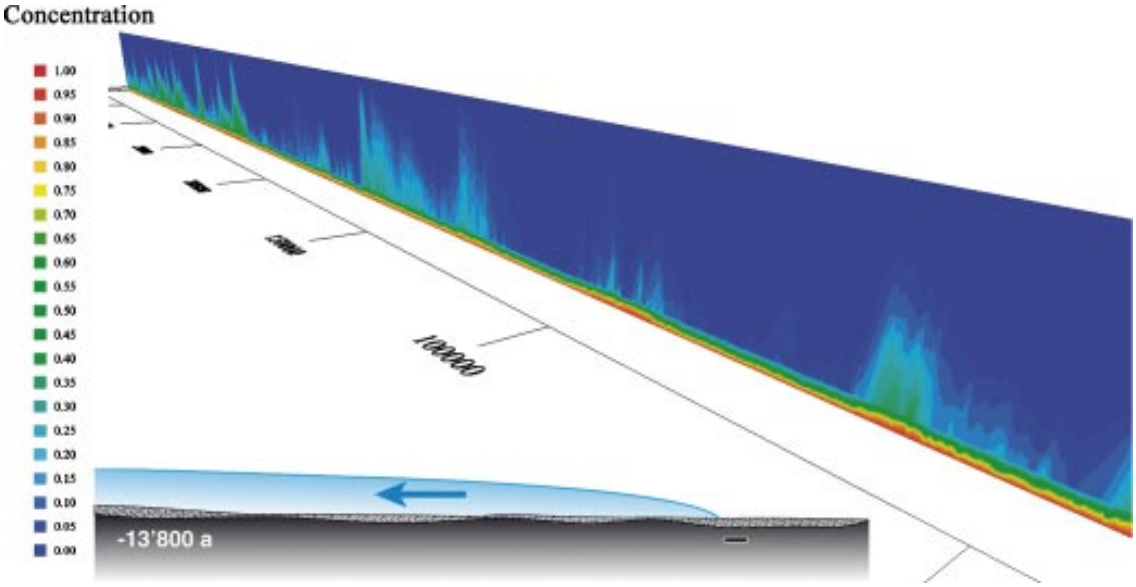

Figure 4-31. *Simulation of the 50 mm case (relative concentration), for time step –13,800 a. The ice margin is located at Y ≈ 100,000 m.*

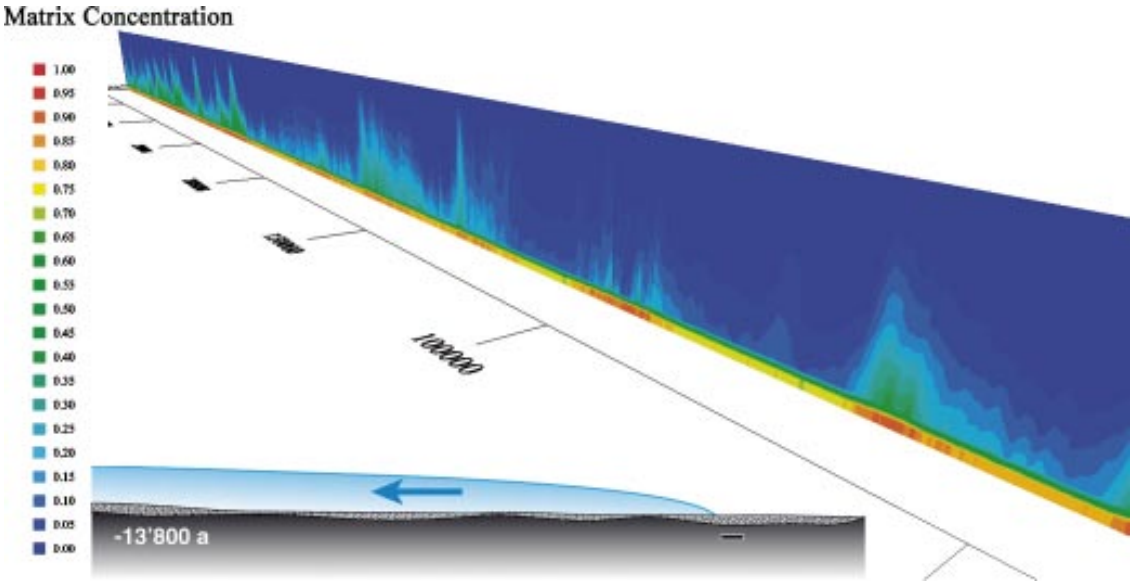

Figure 4-32. *Simulation of the 50 mm case (relative matrix concentration) for the time step –13,800 a. The ice margin is located at Y ≈ 100,000 m.*

For the 50 mm case, the evolution of the flow patterns was also analysed at repository location at a depth of 500 m. The arrival and the retreat of the ice sheet at Simpevarp cause a much smaller increase in the Darcy velocity than in the base case (see Figure 4-33 and Figure 4-20: for the base case, the maximum values for the Darcy velocity are ca 7 to 8 higher than the maximum values of the 50 mm case). This effect is also revealed when comparing, for selected time steps, horizontal cuts at repository level (cf Appendix; Figure A1-1 to Figure A1-10).

The concentration profiles of the 50 mm case exhibit similar shapes as the base case. The phase of glacial build-up with an increase in the concentrations (dominated by diffusive effects) is similar to the base case. When the ice sheet approaches the Simpevarp area, the smaller Darcy velocities cause sufficient advective effects to have meltwater at repository level. Finally, during glacial completeness and glacial retreat, no more variability is observed in concentration. Concentration remains at a low level until the end of the simulation since most of the salinity was flushed out at repository level.

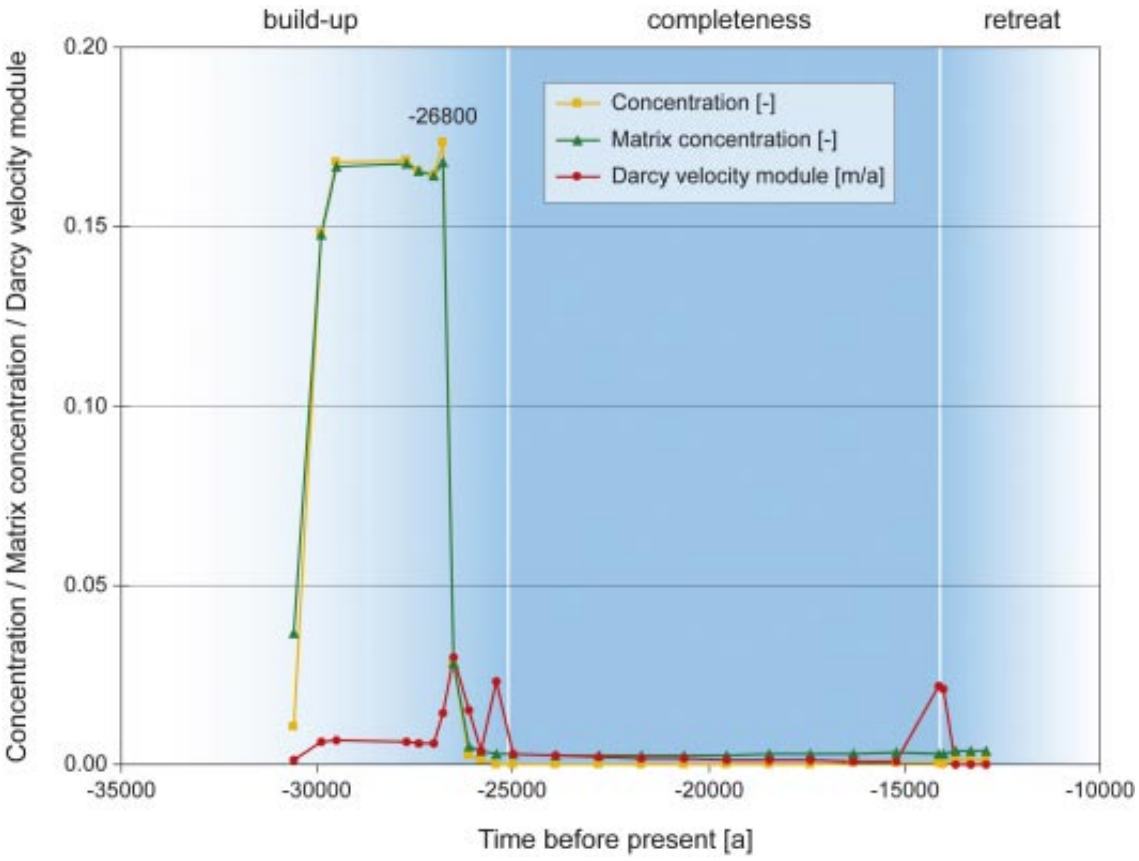

Figure 4-33. *50 mm case: evolution of concentration and Darcy velocity module (expressed in m/a) at repository location (500 m depth) during glacial phases.*

4.5 Particle tracking calculations

Particle tracking calculations were performed to assess performance measures in relation to a hypothetical repository located in the Simpevarp local area. For each of the five specific time steps of the glaciation model (cf Figure 4-4), several thousand particles located in the Simpevarp area (cf Figure 4-1) were started at a depth of 500 m. Performing particle tracking in the steady state mode is acceptable because most of the expected travel times are likely to be shorter than the time steps applied for the glaciation model (cf part 3.5). For the statistical analysis, particles with long trajectories likely to travel within conductive features were removed in order to avoid biased results.

For both the base case and the 50 mm case short travel times were observed with averages (as well as 50th percentile) below 10 a during stages of glacial build-up and glacial retreat (see Table 4-1, Table 4-2, Figure 4-34 and Figure 4-35). The results of particle tracking show some correlation in terms of the location of the ice sheet. In fact, the symmetrical pattern exhibited by the travel times and the F-factors reflects the position of the ice margin with respect to the repository area. The F-factor /Hartley et al. 2005/, $F = \sum_{l} \zeta \, \delta l / \mathrm{q}$, where δl is a step in distance along the path of the particle, characterises transport resistance along the calculated trajectories.

Both during glacial build-up and glacial retreat, when the ice still covers the repository area (i.e. at time steps –26,500 a and –13,900 a) the travel times exhibit similarly low values (for the base case, respectively: 1.4 a and 1.5 a; for the 50 mm case, respectively: 5.2 a and 5.7 a). The same observation is valid when the ice margin is barely upstream of the repository area at –26,800 and –13,800 a (for the base case, respectively: 2.0 a and 1.8 a; for the 50 mm case, respectively: 7.4 a and 6.9 a). The reason is that comparably large amounts of meltwater are released as the ice margin holds a similar position during advance and retreat and, accordingly, the particles travel along similar trajectories. In absolute terms, the average travel times in Table 4-1 and Table 4-2 reflect that the heaviest melting is associated with the periods of glacier build-up and retreat.

Table 4-1. Statistics for particle tracking calculations for the 200 mm case (base case): travel time and F-factor.

Performance measure	Time step	Mean	σ	Q5	Q25	Q50	Q75	Q95	N_traj.[1)]
Travel time log [a]	–26,800[b)]	**0.293**	0.348	–0.223	0.074	*0.257*	0.460	0.888	3,644
	–26,500[b)]	**0.143**	0.381	–0.593	–0.083	*0.110*	0.411	0.780	650
	–17,900[c)]	**3.341**	0.131	3.086	3.299	*3.324*	3.405	3.553	3,062
	–13,900[r)]	**0.182**	0.381	–0.494	–0.050	*0.167*	0.442	0.767	935
	–13,800[r)]	**0.244**	0.340	–0.260	0.047	*0.211*	0.405	0.844	3,645
F–factor Log [a/m]	–26,800[b)]	**4.462**	0.691	3.251	4.008	*4.540*	5.002	5.431	3,644
	–26,500[b)]	**4.260**	0.715	2.915	3.646	*4.508*	4.854	5.090	650
	–17,900[c)]	**6.702**	0.493	5.770	6.410	*6.796*	7.036	7.384	3,062
	–13,900[r)]	**4.439**	0.721	3.006	3.936	*4.735*	4.957	5.254	935
	–13,800[r)]	**4.413**	0.688	3.235	3.953	*4.481*	4.949	5.387	3,645

1) Maximum number of valid trajectories is 3,645.

b) Build-up.

c) Completeness.

r) Retreat.

When comparing the 200 mm and 50 mm cases (see Table 4-1 and Table 4-2), the average travel times for the phases of glacial advance and glacial retreat increase by a factor of about 3 to 4 for the 50 mm case. The reduction of the maximum infiltration to 50 mm leads to lower Darcy velocities and hence to the ca proportional differences observed for the average travel times.

The longest average travel times (2,193 a for the base case and 1,503 a for the 50 mm case) occur during the period of glacial completeness. The difference in the average times should not be taken as relevant since the number of valid trajectories obtained for the 50 mm case was rather low in comparison to the base case. However, the results for glacial completeness must be taken with some caution, as in this case, the only exfiltration zone for the particles is located in the Southern part of the model (see Figure A1-11 in Appendix). This zone is the only one holding boundary conditions with prescribed atmospheric pressure. Everywhere else on the top surface of the model, in the presence of the ice sheet, boundary conditions are provided as (transient) prescribed flow. Therefore, the travel times for particles during glacial completeness are likely to be overestimated.

The F-factor results corresponding to phases of glacial advance and retreat (–26,800 a, –26,500 a, –13,900 a and –13,800 a) are significantly lower in comparison to those for the phase of glacial completeness. This is due to the increased Darcy velocity and shorter travel distance during the phases of glacial advance and retreat. During these glacial phases, when comparing the base case to the 50 mm case, the decrease in the maximum recharge (leading to lower Darcy velocity) is followed by an increase of the average F-factor to about one half order of magnitude. For a given time step, when comparing the base case and the 50 mm case, the histograms of their respective performance measures show similar shapes (see Figure 4-34 and Figure 4-35). The histograms of the remaining time steps are given in Appendix.

When comparing the performance measures of the base case calibrated for the Simpevarp area (see Table 4-3) and the base case of the glaciation model (see Table 4-1; phases of glacial build-up and retreat), the average travel time are more than two orders of magnitude larger and the average F-factor at least one order of magnitude larger in the Simpevarp model for the temperate period.

Table 4-2. Statistics for particle tracking calculations for the 50 mm case: travel time and F-factor.

Performance measure	Time Step	Mean	σ	Q5	Q25	Q50	Q75	Q95	N_traj.[1)]
Travel time log [a]	–26,800[b)]	**0.870**	0.393	0.336	0.622	*0.803*	1.074	1.574	3,644
	–26,500[b)]	**0.717**	0.347	0.003	0.557	*0.711*	0.947	1.267	963
	–17,900[c)]	**3.177**	0.065	3.089	3.144	*3.164*	3.197	3.293	329
	–13,900[r)]	**0.758**	0.374	0.071	0.514	*0.739*	1.030	1.363	854
	–13,800[r)]	**0.840**	0.339	0.329	0.642	*0.805*	1.005	1.442	3,645
F–factor Log [a/m]	–26,800[b)]	**5.011**	0.689	3.780	4.587	*5.086*	5.537	5.928s	3,644
	–26,500[b)]	**4.901**	0.685	3.558	4.392	*5.104*	5.445	5.727	963
	–17,900[c)]	**6.639**	0.408	5.881	6.329	*6.743*	6.936	7.161	329
	–13,900[r)]	**4.962**	0.716	3.596	4.372	*5.287*	5.501	5.804	854
	–13,800[r)]	**5.015**	0.688	3.835	4.555	*5.087*	5.445	5.987	3,645

1) Maximum number of valid trajectories is 3,645.

b) Build-up.

c) Completeness.

r) Retreat.

Table 4-3. Statistics for the base case SReg 4Component IC2 /after Hartley et al. 2005/: travel time and F-factor.

Performance measure	Mean	σ	Q5	Q25	Q50	Q75	Q95
Travel time log [a]	**2.662**	0.768	1.616	2.044	*2.518*	3.249	4.034
F-factor Log [a/m]	**6.061**	0.752	4.973	5.503	*5.939*	6.612	7.390

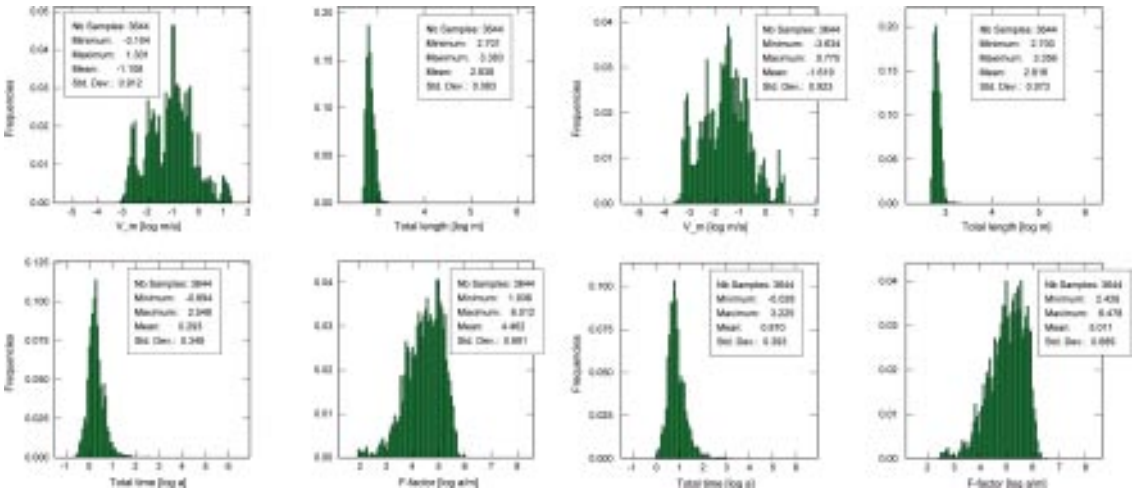

Figure 4-34. *Histograms at time step –26,800 a (glacial build-up) for Darcy velocity (module), path length, travel time and F-factor: base case (left group of 4 histograms) and 50 mm case (right group of 4 histograms).*

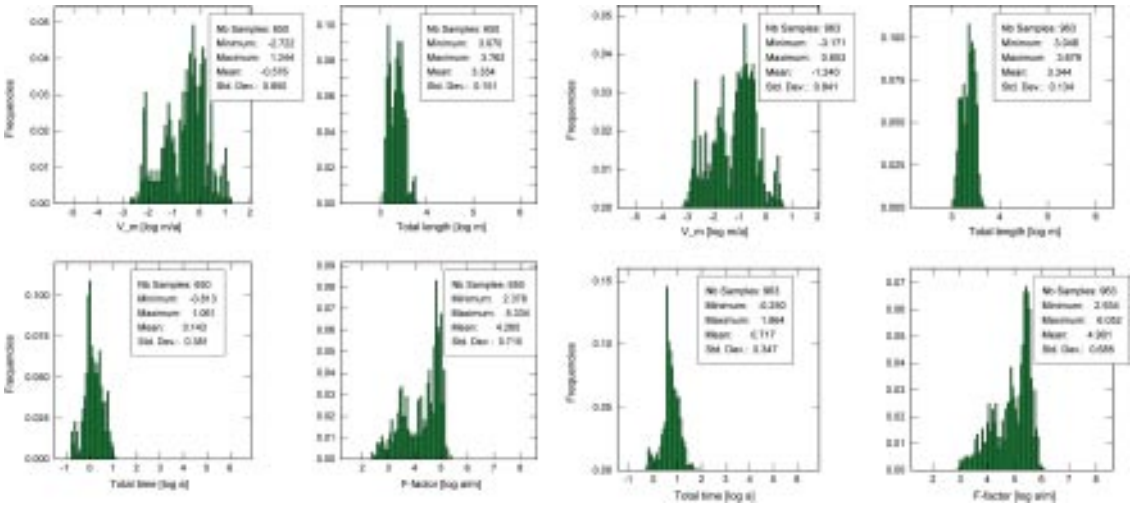

Figure 4-35. *Histograms at time step –26,500 a (glacial build-up) for Darcy velocity (module), path length, travel time and F-factor: base case (left group of 4 histograms) and 50 mm case (right group of 4 histograms).*

5 Conclusions, discussion and perspectives

A groundwater flow model (glaciation model) was developed at a regional scale in order to study long term transient effects related to a glaciation scenario likely to occur in response to climatic changes. The influence of such glacial effects needs to be studied with respect to repository performance and safety as they are believed to induce profound modifications on the groundwater flow patterns.

Conceptually the glaciation model was based on the regional model of Simpevarp and was then extended to a mega-regional scale (of several hundred kilometres) in order to account for the effects of the ice sheet. These effects were modelled using transient boundary conditions provided by a dynamic ice sheet model describing the phases of glacial build-up, glacial completeness and glacial retreat needed for the glaciation scenario.

The results demonstrate the strong impact of the ice sheet on the flow field, in particular during the phases of the build-up and the retreat of the ice sheet. These phases last for several thousand years and may cause large amounts of meltwater to reach the level of the repository and below. The highest fluxes of meltwater are located in the vicinity of the ice margin. As the ice sheet approaches the repository location, the advective effects gain dominance over diffusive effects in the flow field. In particular, up-coning effects are likely to occur at the margin of the ice sheet leading to potential increases in salinity at repository level. For the base case, the entire salinity field of the model is almost completely flushed out at the end of the glaciation period.

The flow patterns are strongly governed by the location of the conductive features in the sub-glacial layer. The influence of these glacial features is essential for the salinity distribution as is their impact on the flow trajectories and, therefore, on the resulting performance measures.

Travel times and F-factor were calculated using the method of particle tracking. Glacial effects cause major consequences on the results. In particular, average travel times from the repository to the surface are below 10 a during phases of glacial build-up and retreat. In comparison to the base case calibrated for the Simpevarp regional model (version 1.2; temperate period), average travel time and F-factor are reduced by about two orders and one order of magnitude, respectively, for phases of ice sheet displacement.

In order to evaluate the effects of the maximum recharge, a sensitivity case was performed with a maximum recharge equal to 50 mm/a, i.e. a reduction by a factor 4 with respect to the base case. This sensitivity case shows perturbations in the flow patterns due to glacial effects, although to a lesser extent than in the base case. In terms of performance measures, the 50 mm/a case presents increases in travel time (ca factor 3 to 4) and F-factor (about one half order of magnitude) as compared to the base case during phases of build up and retreat. In other words, the penetration depth of the meltwater is still well below the level of the repository. Thus, at this level, up-coning effects are expected during phases of ice sheet displacement.

The following recommendations regarding further work on open issues may be postulated:

1. Investigations of the conceptual uncertainty linked to the sub-glacial layer. Alternative concepts are currently under study by SKB glaciologists. One concept in particular considers the replacement of the transient flow boundary with a transient head boundary with the values depending on the ice sheet thickness and head drawdowns being specified at the locations of the conductive features. Another option would be to apply a mix of time-dependent boundary conditions; i.e. to use a prescribed flux dynamically constrained by the ice-sheet thickness from one time step to the next /Lemieux 2006/. This type of boundary would allow the computation of subglacial infiltration in a more realistic manner.

2. Assessment of the impact of a lower value for the flow wetted surface with respect to the concentration fields and the performance measures.

   First estimates of the characteristic diffusion time reveal that instantaneous equilibrium between the concentration of the flowing fractures and the rock matrix is no longer likely to occur which could lead to additional transport of salinity.

3. Evaluation of geomechanical effects and permafrost conditions through the application of temporally variable hydraulic parameters related to the location of the ice sheet.

   Geomechanical effects due to ice loading are likely to induce modifications in the groundwater flow field. In terms of rock deformation, the impact of the ice sheet loading leads to variations in porosity, hydraulic conductivity and pore pressure. The modelling of groundwater flow (with geomechanical effects) should be initiated with scoping calculations of hydromechanical coupling following the approach of /Lemieux 2006/.

   During the progression of the ice sheet, permafrost is formed within several kilometres of its perimeter. The permafrost greatly reduces the hydraulic conductivity. The importance of the permafrost relates to the location of the ice sheet and needs to be evaluated with respect to repository performance.

4. Application of a novel methodology for the determination of groundwater age, life expectancy and transit time distributions.

   This methodology developed by /Cornaton and Perrochet 2005ab/ allows to avoid numerical problems inherent to particle tracking methods when used in combination with finite elements. It may be a valuable alternative, but it would first require some testing, e.g. at the scale of the S1.2 regional model.

   The modelling approach applied for the study of a glaciation scenario at Simpevarp has successfully described the assumed conditions and some of the relevant processes. It may certainly serve as a well founded base for future modelling tasks to provide solutions to further questions.

6 References

Carrera J, Sanchez-Vila X, Benet I, Medina A, Galarza G, Guimera J, 1998. On matrix diffusion: formulations, solutions methods and quantitative effects, Hydrogeology Journal, 6, 1, 178–190.

Chilès J P, Delfiner P, 1999. Geostatistics: modelling spatial uncertainty, Wiley Series in Probability and Mathematical Statistics, 695p.

Cornaton F, Perrochet P, 2005a. Groundwater age, life expectancy and transit time distributions in advective-dispersive systems: 1. Generalised reservoir theory, Advances in Water Resources, in press.

Cornaton F, Perrochet P, 2005b. Groundwater age, life expectancy and transit time distributions in advective-dispersive systems: 2. Reservoir theory for sub-drainage basins, Advances in Water Resources, in press.

Hartley L, Woth D, Gylling B, Marsic N, Holmén J, 2004. Preliminary site description: groundwater flow simulations, Simpevarp area (version 1.1) modelled with ConnectFlow, SKB R-04-63, Svensk Kärnbränslehantering AB.

Hartley L, Hoch A R, Hunter F, Jackson C P, 2005. Regional hydrogeological simulations – Numerical modelling using ConnectFlow, Preliminary site description Simpevarp sub area – version 1.2, SKB R-05-12, Svensk Kärnbränslehantering AB.

Hoch A R, Jackson C P, 2004. Rock-matrix diffusion in transport of salinity, SKB R-04-78, Svensk Kärnbränslehantering AB.

Jaquet O, Siegel P, 2003. Groundwater flow and transport modelling during a glaciation period, SKB R-03-04, Svensk Kärnbränslehantering AB.

Jaquet O, Siegel P, 2004. Local-scale modelling of density-driven flow for the phases of repository operation and post-closure at Beberg, SKB R-04-46, Svensk Kärnbränslehantering AB.

Jaquet O, Siegel P, Klubertanz G, Benabderrhamane H, 2004. Stochastic discrete model of karstic networks, Advances in Water Resources, 27, 751–760.

Lemieux J M, 2006. Impact of the Wisconsinian glaciation on Canadian continental groundwater flow, PhD Thesis, University of Waterloo, Canada.

Marsic N, Hartley L, Jackson P, Poole M and Morvik A, 2001. Development of hydrogeological modelling tools based on NAMMU, SKB TR-01-49, Svensk Kärnbränslehantering AB.

Marsic N, Hartley L, Sanchez-Friera P, Morvik A, 2002. Embedded regional/local-scale model of natural transients in saline groundwater flow illustrated using the Beberg site, SKB R-02-22, Svensk Kärnbränslehantering AB.

Näslund J O, Fastook J, 2005. Metadata for nested high resolution (10 km) ice sheet model run of 24th March 2005, Stockholm University.

Näslund J O, 2004. Personal communication.

Paterson W S B, 1994. The physics of glaciers, Pergamon Press, Oxford, 3rd edition.

SKB, 2006. Climate and climate related issues for the safety assessment SR-Can, SKB TR-06-23, Svensk Kärnbränslehantering AB.

Svensson U, 1999. Subglacial groundwater flow at Äspö as governed by basal melting and ice tunnels, SKB R-99-38, Svensk Kärnbränslehantering AB.

Thomsen H H, Thorning L, Braithwaite R, 1989. Applied glacier research for planning hydro-electric power, Ilulissat/Jakobshavn, West Greenland. Annals of Glaciology, 13: 257–261.

Wackernagel H, 2003. Multivariate Geostatistics, 3rd edition, Springer, Berlin.

Walker D, Rhén I, Gurban I, 1997. Summary of hydrogeologic conditions at Aberg, Beberb and Ceberg, SKB TR-97-23, Svensk Kärnbränslehantering AB.

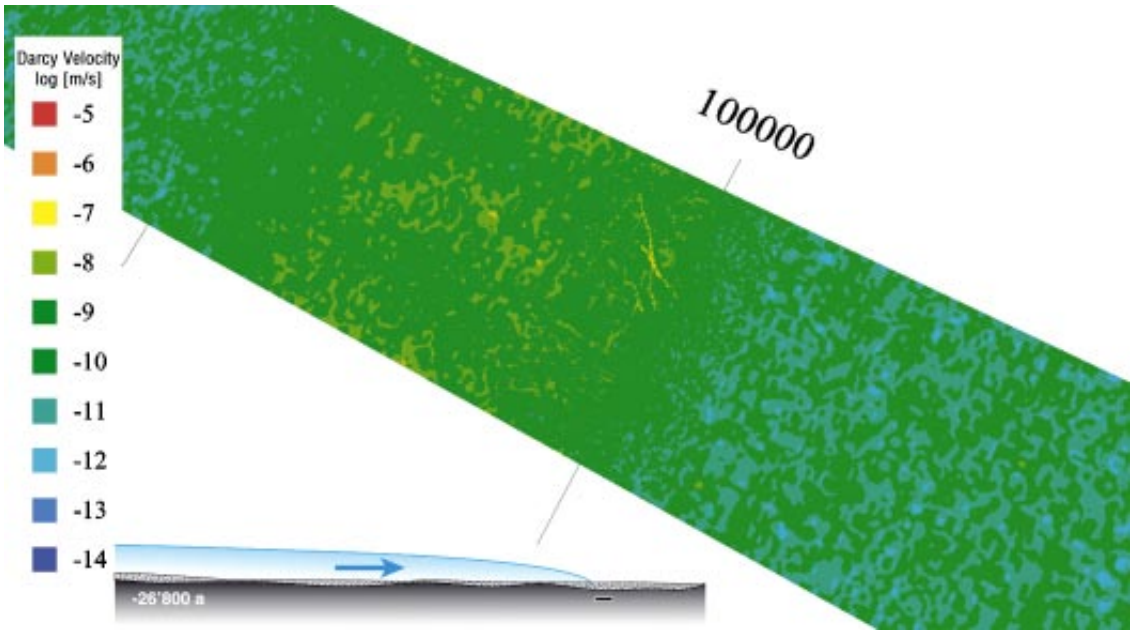

Figure A1-1. *Base case: Darcy velocity (module) field for time step –26,800 a, horizontal cut at depth of 500 m.*

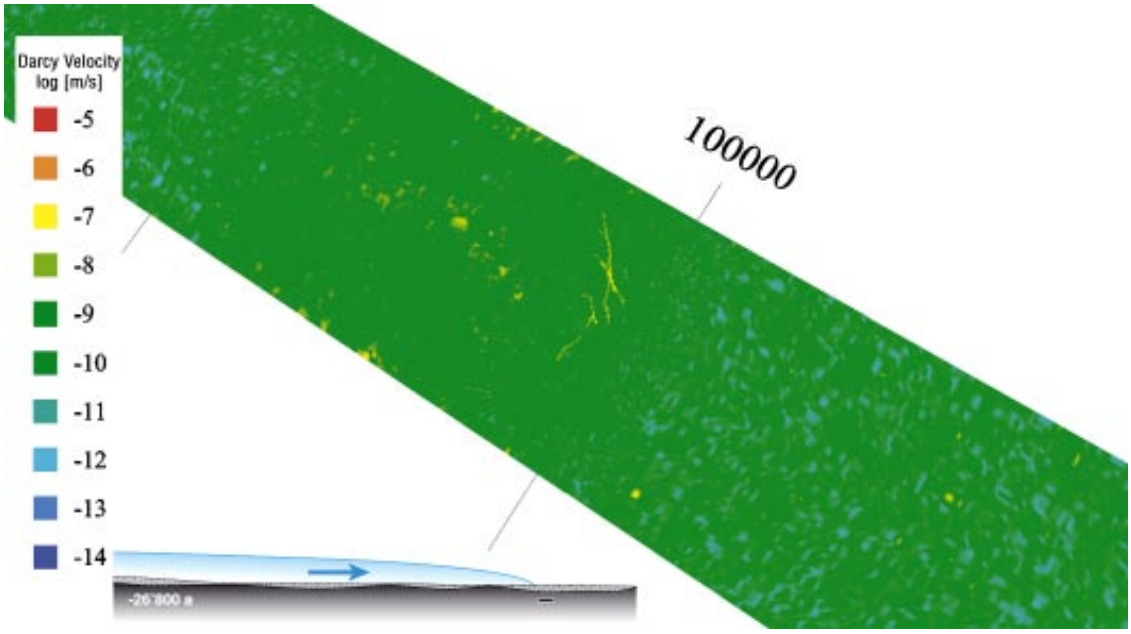

Figure A1-2*. 50 mm case: Darcy velocity field (module) for time step –26,800 a, horizontal cut at depth of 500 m.*

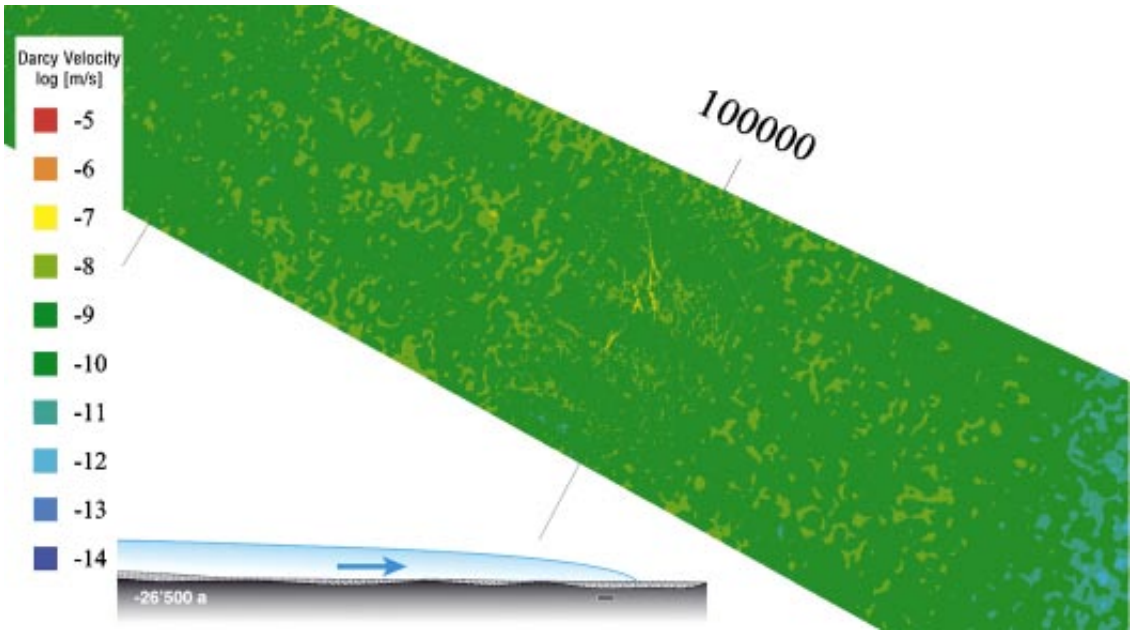

Figure A1-3. *Base case: Darcy velocity (module) field for time step –26,500 a, horizontal cut at depth of 500 m.*

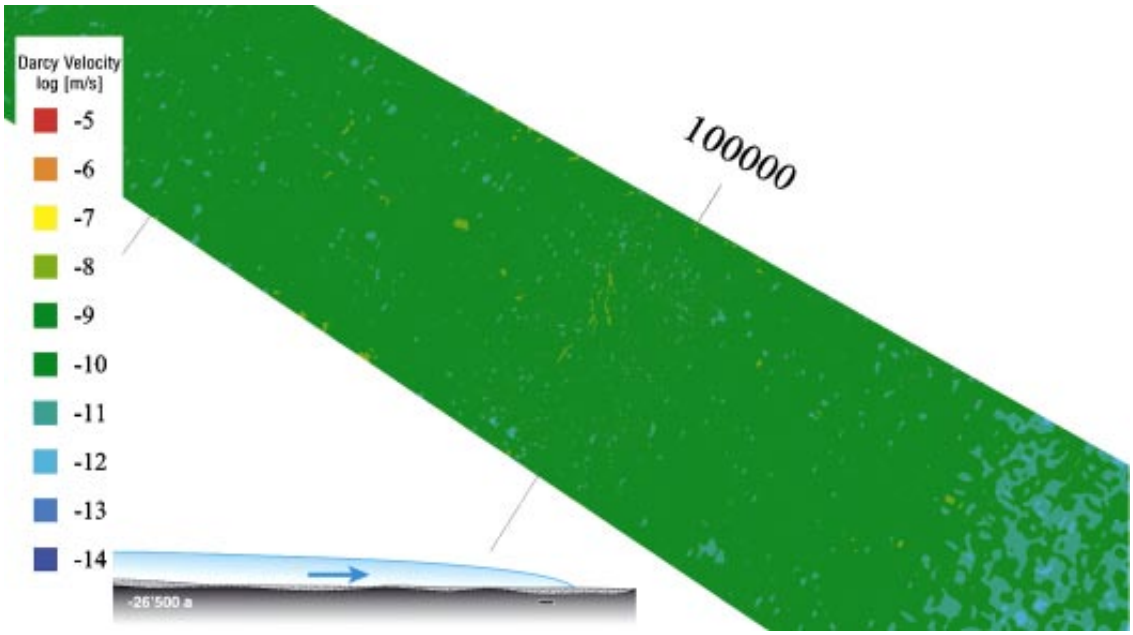

Figure A1-4. *50 mm case: Darcy velocity (module) field for time step –26,500 a, horizontal cut at depth of 500 m.*

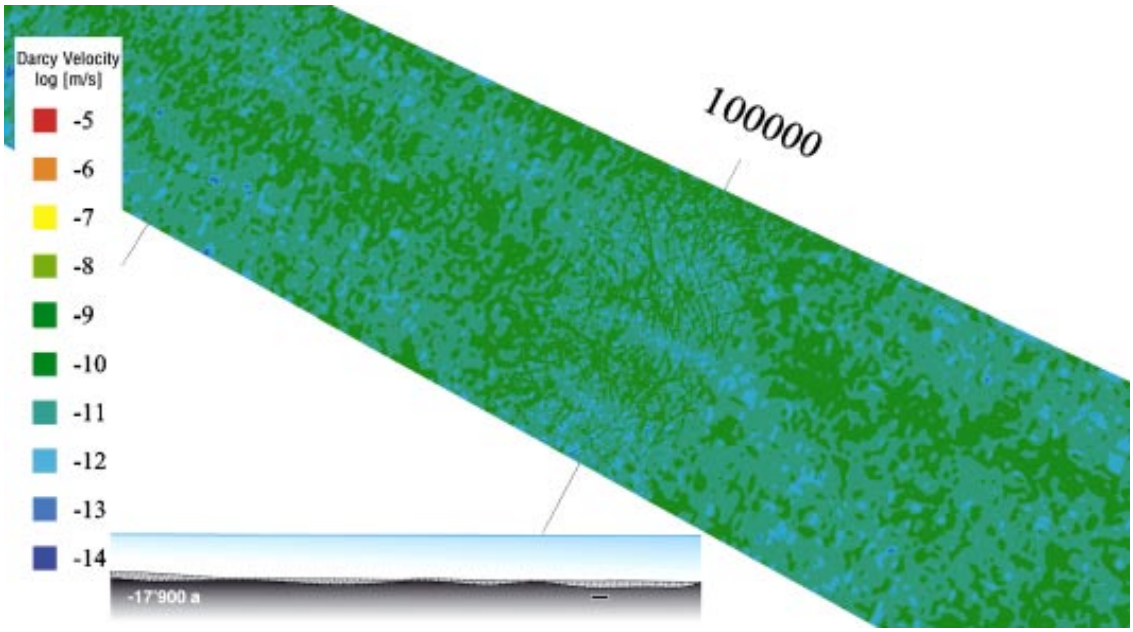

Figure A1-5. *Base case: Darcy velocity (module) field for time step –17,900 a, horizontal cut at depth of 500 m.*

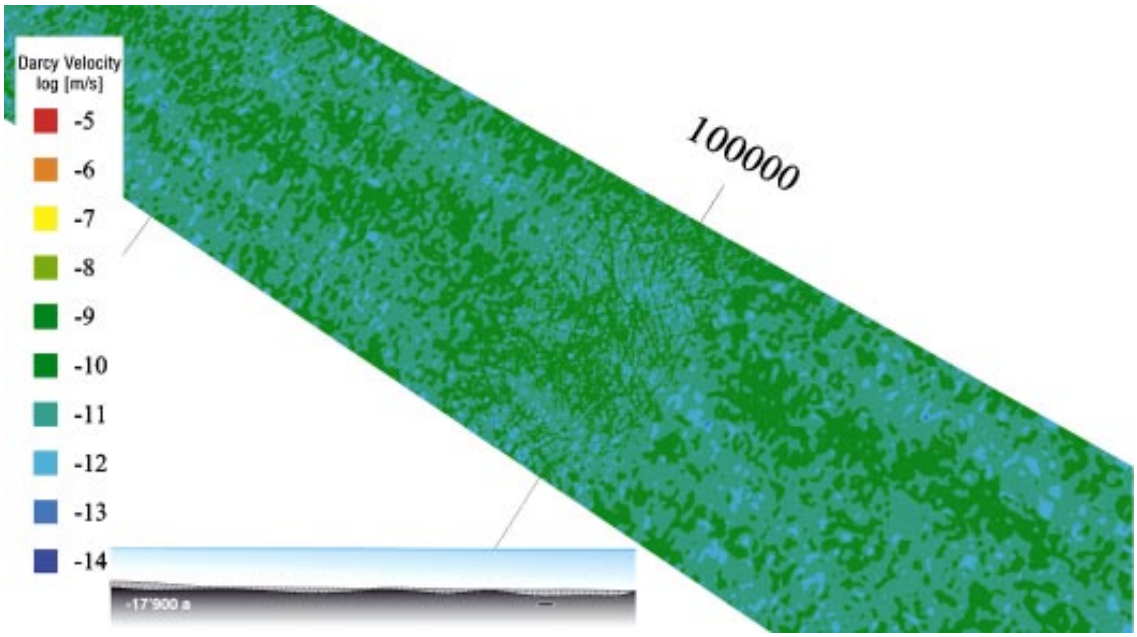

Figure A1-6. *50 mm case: Darcy velocity (module) field for time step –17,900 a, horizontal cut at depth of 500 m.*

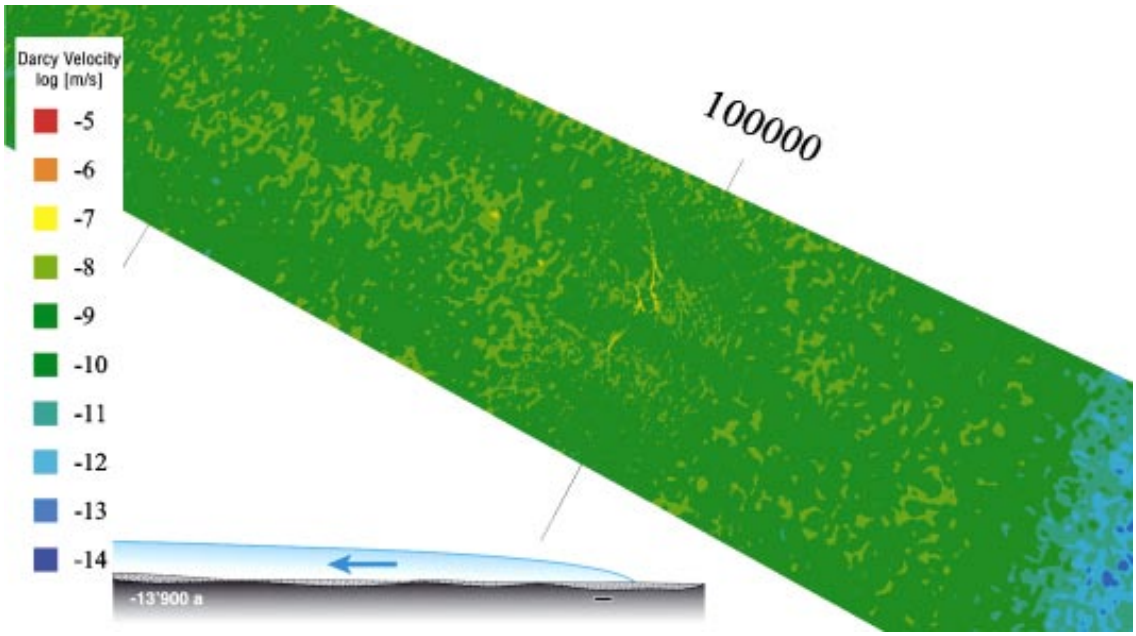

Figure A1-7. *Base case: Darcy velocity (module) field for time step –13,900 a, horizontal cut at depth of 500 m.*

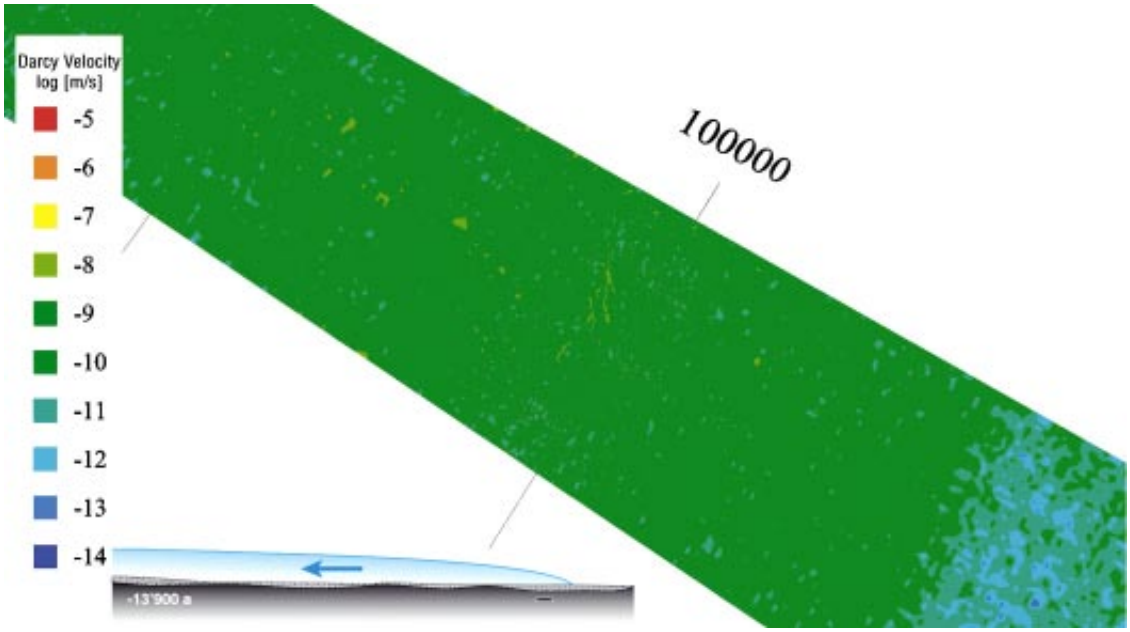

Figure A1-8. *50 mm case: Darcy velocity (module) field for time step –13,900 a, horizontal cut at depth of 500 m.*

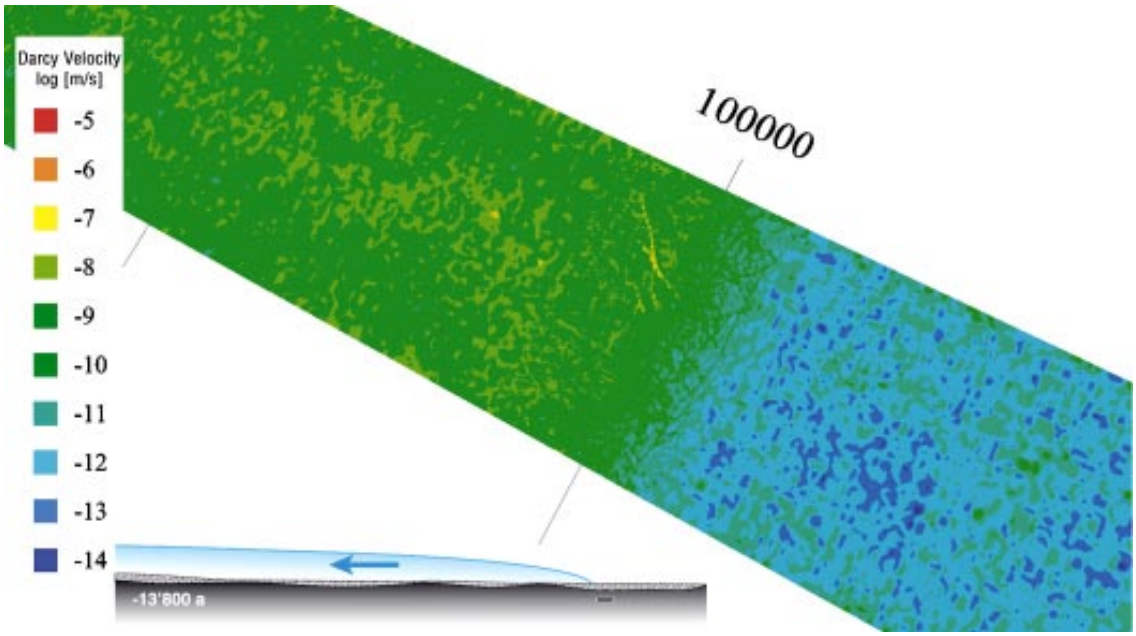

Figure A1-9. *Base case: Darcy velocity (module) field for time step –13,800 a, horizontal cut at depth of 500 m.*

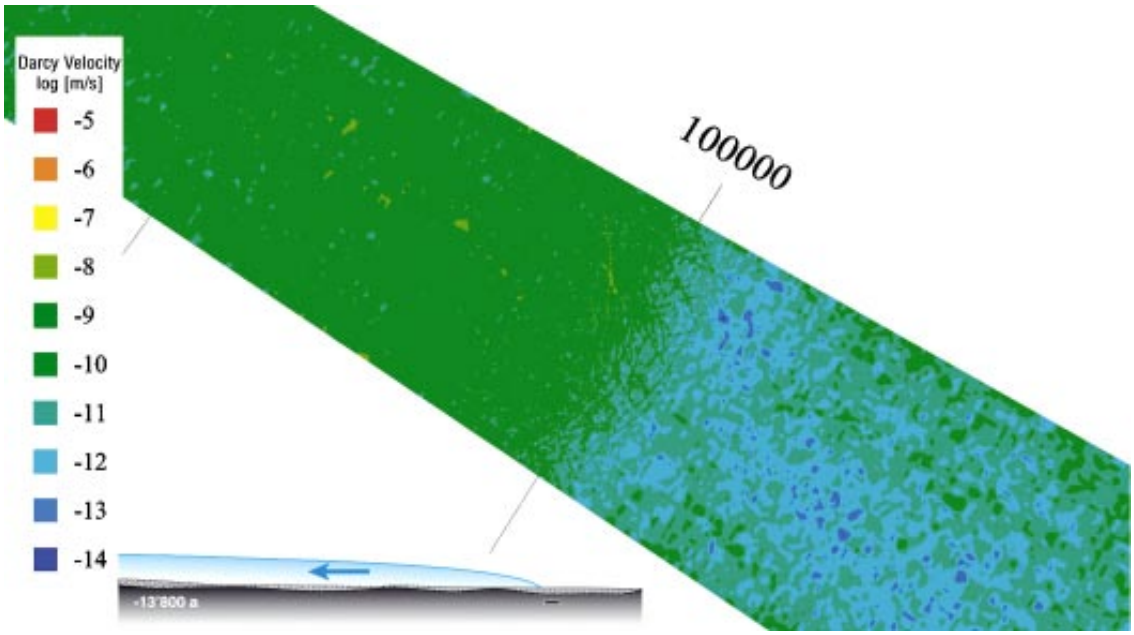

Figure A1-10. *50 mm case: Darcy velocity (module) field for time step –13,800 a, horizontal cut at depth of 500 m.*

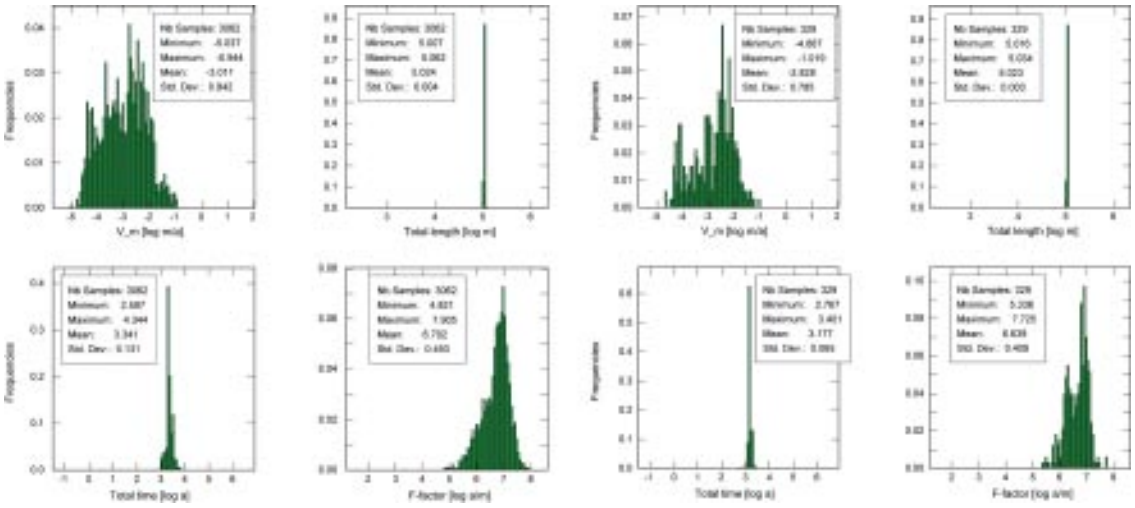

Figure A1-11. *Histograms at time step –17,900 a (glacial completeness) for Darcy velocity (module), path length, travel time and F-factor: base case (left group of 4 histograms) and 50 mm case (right group of 4 histograms).*

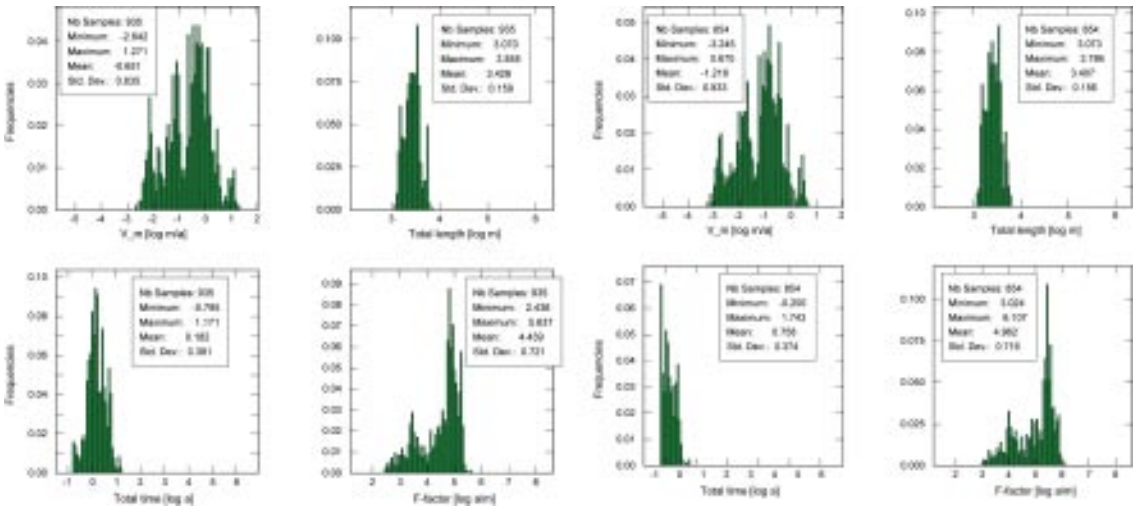

Figure A1-12. *Histograms at time step –13,900 a (glacial retreat) for Darcy velocity (module), path length, travel time and F-factor: base case (left group of 4 histograms) and 50 mm case (right group of 4 histograms).*

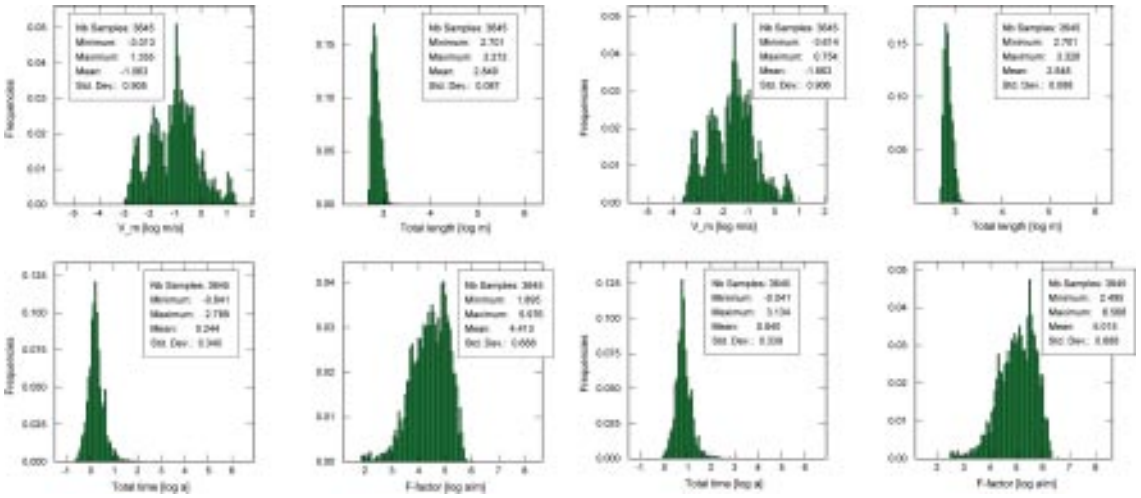

Figure A1-13. *Histograms at time step –13,800 a (glacial retreat) for Darcy velocity (module), path length, travel time and F-factor: base case (left group of 4 histograms) and 50 mm case (right group of 4 histograms).*